High-dimensional analysis reveals a distinct population of adaptive-like tissue-resident NK cells in human lung

Nicole Marquardt[1*], Marlena Scharenberg[1], Jeffrey E. Mold[2], Joanna Hård[2], Eliisa Kekäläinen[3,4], Marcus Buggert[1], Son Nguyen[5,6], Jennifer N. Wilson[1], Mamdoh Al-Ameri[7], Hans-Gustaf Ljunggren[1], Jakob Michaëlsson[1]

Running title: Adaptive-like human lung tissue-resident NK cells

Affiliations:

[1]Center for Infectious Medicine, Department of Medicine, Karolinska Institutet, Stockholm, Sweden

[2]Department of Cell and Molecular Biology, Karolinska Institutet, Stockholm, Sweden

[3]Translational Immunology Research Program & Department of Bacteriology and Immunology, University of Helsinki, Finland

[4]HUSLAB, Division of Clinical Microbiology, Helsinki University Hospital, Helsinki, Finland,

[5]Department of Microbiology, Perelman School of Medicine, University of Pennsylvania, Philadelphia, PA, USA

[6]Institute for Immunology, Perelman School of Medicine, University of Pennsylvania, Philadelphia, PA, USA

[7]Thoracic Surgery, Department of Molecular Medicine and Surgery, Karolinska Institutet, Karolinska University Hospital, Stockholm, Sweden

25 ***Corresponding author:** Nicole Marquardt, Center for Infectious Medicine,
26 Department of Medicine, Karolinska Institutet, Karolinska University Hospital, 141 86
27 Stockholm, Sweden; E-mail: nicole.marquardt@ki.se, Phone: +46-8-58589791 Fax:
28 +468-7467637

Abstract

The concept of adaptive-like "memory" NK cells has been extensively investigated in recent years. In humans, NK cells with adaptive-like features have been identified in peripheral blood and liver of cytomegalovirus (CMV)-seropositive individuals. The human lung is a major target organ for infections and is also a significant reservoir for CMV. However, it remains unknown whether adaptive-like NK cells can be found in this organ. Using RNAseq and flow cytometry analysis, we here identify a novel adaptive-like $KIR^{+}NKG2C^{+}$ NK cell subset with a $CD49a^{+}CD56^{bright}CD16^{-}$ tissue-resident (tr)NK cell phenotype in human lung and in peripheral blood. Adaptive-like lung trNK cells were found to be present independently of adaptive-like $CD56^{dim}CD16^{+}$ NK cells, to be hyperresponsive towards target cells, and to exhibit signs of metabolic reprogramming. In conclusion, adaptive-like trNK cells constitute a novel subset of human lung NK cells, likely contributing to unique defense mechanisms in context of infection at this site.

Key words: NK cells, adaptive, lung, tissue-resident

Abbreviations:

Eomes: Eomesodermin

FITC: Fluorescein isothiocyanate

HCMV: Human cytomegalovirus

ILC: Innate lymphoid cell

KIR: Killer cell immunoglobulin-like receptor

NK: Natural killer

PE: Phycoerythrin

ROS: Reactive oxygen species

Introduction

Natural killer (NK) cells are a crucial part of the innate immune system. They eliminate virus-infected and malignant cells, and produce proinflammatory cytokines including IFN-γ and TNF. In recent years, the concept of adaptive-like or "memory" NK cells has emerged from studies in mice[1-4] and humans[5-10]. These cells share a distinct phenotype and increased target cell responsiveness as well as having features of longevity [11].

Most studies of human adaptive-like NK cells have focused on subsets of NKG2C$^+$(KIR$^+$)CD56^{dim}CD16$^+$ NK cells, originally found to be expanded and stably imprinted in peripheral blood of approximately 30-40% of human CMV (HCMV)-seropositive individuals[5,10]. Adaptive-like CD56^{dim}CD16$^+$ NK cells in human peripheral blood have a distinctive phenotypic[5,10], epigenetic[8,9], and functional[8-10] profile compared to conventional NK cells and have been suggested to contribute to immunity against HCMV[1,12]. We recently described a subset of tissue-resident CD49a$^+$KIR$^+$NKG2C$^+$CD56^{bright}CD16$^-$ NK cells in the human liver[7], potentially representing a counterpart to the CD49a$^+$DX5$^-$ adaptive-like tissue-resident NK (trNK) cells in murine liver. In virus-independent settings, murine hepatic CD49a$^+$DX5$^-$ adaptive-like NK cells have been shown to mediate contact hypersensitivity[3]. Virus-driven antigen-specific NK cell memory has been identified in mouse models following infection with MCMV[1,13,14], influenza A virus (IAV)[4,15,16], vesicular stomatitis virus (VSV)[4], vaccinia virus[17], HIV-1[4], and herpes simplex virus 2 (HSV-2)[16], and after immunization with simian immunodeficiency virus (SIV) in rhesus macaques[18]. Together, current data indicate that viral infections might drive and shift the development of unique NK cell subsets in different compartments.

The human lung is a frequent site of acute infections, including infections with viruses such as influenza virus, respiratory syncytial virus (RSV), and HCMV, as well as serving as a reservoir for latent HCMV infection[19]. Although human CD56^{dim}CD16^{+} lung NK cells are hyporesponsive to *ex vivo* target cell stimulation[20], exposure of NK cells to virus-infected cells is likely to result in functional NK cell priming. Indeed, increased polyfunctional responses have been observed in CD16^{-} lung NK cells following *in vitro* infection with IAV[21,22].

Here, we identify a novel adaptive-like CD49a^{+}KIR^{+}NKG2C^{+}CD56^{bright}CD16^{-} NK cell population in the human lung with a tissue-resident phenotype. In donors with expansions of adaptive-like lung trNK cells, small but detectable frequencies of similar NK cells were detected in paired peripheral blood. While adaptive-like KIR^{+}NKG2C^{+}CD56^{dim}CD16^{+} NK cells (as commonly identified in peripheral blood of HCMV-seropositive donors) and CD49a^{+}KIR^{+}NKG2C^{+}CD56^{bright}CD16^{-} adaptive-like lung and blood NK cells shared a common core gene signature, we identified several unique features of each population indicating that they may represent separate developmental lineages. Notably, NK cells from donors with an adaptive-like trNK cell expansion in the lung were hyperresponsive towards target cells and expressed gene sets enriched for metabolic reprogramming. Together, CD49a^{+}KIR^{+}NKG2C^{+}CD56^{bright}CD16^{-} trNK cells in the human lung represent a novel lineage of adaptive-like NK cells with potentially significant implications in lung surveillance and lung-associated pathologies.

Results

Adaptive-like NK cells can be identified in human lung

We first set out to investigate whether expansions of $KIR^{+}NKG2C^{+}$ adaptive-like NK cells could be identified in the human lung. The majority of NK cells in the lung are phenotypically similar to NK cells found in peripheral blood ($CD69^{-}CD56^{dim}CD16^{+}$), suggesting that these cells may recirculate between this organ and peripheral blood[20]. Accordingly, $KIR^{+}NKG2C^{+}CD56^{dim}CD16^{+}$ NK cells could be identified not only in peripheral blood but also in the lung (Fig. 1a). Surprisingly, KIR and NKG2C were also co-expressed on $CD56^{bright}CD16^{-}$ lung NK cells, with varying frequencies between donors (Fig. 1b, c) (see Supplementary Fig. 1a for the gating strategy to identify $KIR^{+}NKG2C^{+}CD56^{bright}CD16^{-}$ and $CD56^{dim}CD16^{+}$ NK cells). In several donors the frequencies of $KIR^{+}NKG2C^{+}CD56^{bright}CD16^{-}$ NK cells in human lung vastly exceeded those previously described in the liver[7], with up to 98% of $CD56^{bright}CD16^{-}$ lung NK cells co-expressing KIR and NKG2C (Fig. 1 a, b).

Next, we assessed phenotypic features of $KIR^{+}NKG2C^{+}CD56^{bright}CD16^{-}$ lung NK cells in an unbiased manner. Uniform manifold approximation and expression (UMAP) analysis revealed a distinct subset of cells with an expression pattern consistent with adaptive-like NK cells found in peripheral blood and liver, including low expression of Siglec-7 and CD161, and high expression of NKG2C, KIRs, and CD2[7,8,23,24] (Fig. 1d). Unlike $KIR^{+}NKG2C^{+}CD56^{dim}CD16^{+}$ NK cells, $KIR^{+}NKG2C^{+}CD56^{bright}CD16^{-}$ NK cells expressed lower levels of CD45RA and NKp80, and higher levels of CD8 (Fig. 1d). In addition to these expression patterns, manual analysis of individual samples additionally confirmed low expression of ILT2 and FcεR1γ, as compared to $KIR^{+}NKG2C^{+}CD56^{dim}CD16^{+}$ lung NK cells (Fig. 1e, f). Furthermore, $KIR^{+}NKG2C^{+}CD56^{bright}CD16^{-}$ lung NK cells displayed higher

expression of Eomes and NKG2A, but no significant differences in T-bet expression. Together, our data reveal the presence of a unique adaptive-like NK cell subset, herein identified as KIR^{+}NKG2C^{+}CD56^{bright}CD16^{-}, in the human lung, which is distinct from adaptive-like CD56^{dim}CD16^{+} NK cells previously described in peripheral blood.

Adaptive-like NK cell expansions in human lung are tissue-resident

Tissue-resident NK cells in human lung are characterized by expression of CD69 and the integrins CD49a and CD103[21,25]. Strikingly, the vast majority of the distinct population of NKG2C^{+}CD56^{bright}CD16^{-} NK cells identified by UMAP analysis co-expressed CD69 (80%) and CD49a (77%), and a substantial proportion (38%) also co-expressed CD103 (Fig. 2a, b), suggesting that this population represented an adaptive-like trNK cell subset. KIR^{+}NKG2C^{+} NK cells co-expressing any of these markers were mainly CD56^{bright}CD16^{-} (Fig. 2c, d), further demonstrating that they are clearly distinct from adaptive-like CD56^{dim}CD16^{+} NK cells.

To further characterize adaptive-like trNK cells in the lung we compared the gene expression profiles of sorted adaptive KIR^{+}NKG2C^{+} and non-adaptive KIR^{-} NKG2C^{-} trNK cells in human lung using RNA sequencing (Fig. 2e, f; see sorting strategy in Supplementary figure 1b, c). 102 genes were differentially expressed ($p<0.05$, log2FC>1), including several *KIR* genes, *CD8A*, *GPR183, IRF8* and *SH2D1B* (EAT2), and genes encoding for the transcription factors MafF (*MAFF*) and ZNF498 (*ZSCAN25*). GPR183 has been demonstrated to be crucial for tissue-specific migration of innate lymphoid cells[26], while EAT2 expression has previously been shown to be downregulated in adaptive-like CD56^{dim}CD16^{+} NK cells[8]. Interestingly, while upregulation of both *IRF8* and *THEMIS2* has been reported to be essential for NK cell-mediated responses against MCMV infection[27,28], gene expression of both molecules

was low in adaptive-like trNK cells in human lung (Fig. 2e). Furthermore, approximately one third of the differentially expressed genes in adaptive-like lung trNK cells were also differentially expressed in adaptive-like CD57^{+}NKG2C^{+}CD56^{dim}CD16^{+} NK cells in peripheral blood (GSE117614)[29], including *KLRC2* (NKG2C), *KLRC3* (NKG2E), *IL5RA*, *GZMH*, *ITGAD* (CD11d), *RGS9*, *RGS10*, and *KLRB1* (CD161), *KLRC1* (NKG2A), *KLRF1* (NKp80), *TMIGD2*, *IL18RAP*, *FCER1G*, *MLC1*, *CLIC3* and *TLE1* (Fig. 2f).

Adaptive-like NK cells in peripheral blood and in the human liver commonly have a distinct KIR expression profile which is dominated by KIRs that bind to self-HLA class I (self-KIRs)[7,10,30]. In the lung, analysis of single KIR expression on CD16^{-} and CD16^{+} NK cell subsets in donors with high frequencies of adaptive-like lung trNK cells revealed that the latter subset displays unique KIR expression patterns compared to CD16^{+} NK cells in blood or lung (Fig. 2g-i; Supplementary Fig. 1d for the gating strategy). High expression of KIRs on the adaptive-like trNK cells was limited to self-KIR, identical to the phenotype described for adaptive-like NK cells in liver and peripheral blood. Notably, even in a donor with adaptive-like NK cell expansions of both trNK cells and CD56^{dim}CD16^{+} NK cells (Fig. 2g), the KIR-expression profile differed between the two subsets.

Together, CD49a^{+}KIR^{+}NKG2C^{+}CD56^{bright}CD16^{-} trNK cells in the human lung exhibit a unique profile of activating and inhibitory NK cell receptors (e.g. NKG2A, KIR, NKp80), as well as adaptor, signaling, and effector molecules (FcεR1γ, SH2D1B, granzyme H). This indicates that these are bona fide adaptive-like trNK cells distinct from adaptive-like CD56^{dim}CD16^{+} NK cells, demonstrating the presence of a yet unexplored NK cell population in the human lung.

Lung adaptive-like trNK cells are hyperresponsive to target cells

In order to determine whether adaptive-like lung trNK cells differ from non-adaptive CD49a$^-$KIR$^-$NKG2C$^-$CD56^{bright}CD16$^-$ lung trNK cells, we compared expression levels of genes associated with functional competence (Fig. 3a). Gene expression in adaptive-like trNK cells was higher for *IFNG*, *IL33*, *XCL1* and *GZMH* (granzyme H), and lower for *GNLY* (granulysin), *GZMA* (granzyme A), *GZMK* (granzyme K), *IL2RB* (CD122) and *IL18RAP* as compared to non-adaptive lung trNK cells (Fig. 3a).

On the protein level, expression levels of perforin were similar in non-adaptive and adaptive-like trNK cells (Fig. 3b, c), consistent with previous results comparing CD49a$^-$ and CD49a$^+$ lung NK cells[25]. In contrast, adaptive-like trNK cells expressed elevated levels of granzyme B as compared to non-adaptive trNK cells (Fig. 3b, c). Expression of granzyme B in adaptive-like trNK cells indicated a potential cytotoxic function in this particular subset, despite lung NK cells generally being characterized as hyporesponsive to target cell stimulation[20,21]. Intriguingly, NK cells from donors with an expansion of adaptive-like trNK cells in the lung degranulated stronger and produced more TNF compared to those from donors without such expansions (Fig. 3d). In particular NK cells co-expressing CD49a and KIR degranulated strongly and produced high levels of TNF upon target cell stimulation (Fig. 3d-f). This hyperresponsiveness of adaptive-like lung trNK cells was independent from co-expression of CD103, since similar activation levels were observed between CD49a$^+$CD103$^-$ and CD49a$^+$CD103$^+$ KIR$^+$NKG2C$^+$ NK cells (Fig. 3f-h). Blood NK cells from donors with expanded adaptive-like lung trNK cells also responded stronger to target cells as compared to donors without such expansions (Fig. 3f-h). Taken together, these results revealed that the presence of expanded adaptive-like trNK cells in the lung is linked to

hyperresponsivity towards target cells, implicating a role of these cells in active immune regulation within the lung.

Adaptive-like CD49a^{+}KIR^{+}NKG2C^{+}CD56^{bright}CD16^{-} NK cells can be identified in matched peripheral blood

As a hallmark of tissue-resident cells, CD49a is commonly expressed on subsets of T cells and NK cells in diverse non-lymphoid compartments such as the lung[21,22,25,31], liver[7], skin[32], uterus[33], intestine[34], but not in peripheral blood. Intriguingly, however, we identified a small subset of CD49a^{+}KIR^{+}NKG2C^{+} NK cells within the CD16^{-} NK cell population in peripheral blood of donors harboring expansions of adaptive-like trNK cells in the lung (Fig. 4a, b). The frequencies of CD49a^{+}KIR^{+}NKG2C^{+}CD16^{-} NK cells in peripheral blood were considerably lower as compared to adaptive-like lung trNK cells and adaptive-like CD56^{dim}CD16^{+} lung and blood NK cells, respectively (Fig. 4b). However, we identified expansions as outliers also in CD49a^{+}KIR^{+}NKG2C^{+}CD16^{-} blood NK cells (Fig. 4b; see gating strategy in Supplementary Fig. 1e). In detail, we found that 18.6% and 25.6% of all donors had an expansion of adaptive-like trNK cells in lung and CD49a^{+}KIR^{+}NKG2C^{+}CD16^{-} NK cells in peripheral blood, respectively. In comparison, 20.9% and 15.1% of all donors had an expansion of adaptive-like CD56^{dim}CD16^{+} NK cells in lung and blood, respectively (Fig. 4b). Interestingly, expansions of adaptive-like CD56^{bright}CD16^{-} and CD56^{dim}CD16^{+} NK cells were virtually mutually exclusive in donors (Fig. 4c). However, there was a substantial overlap within each of these subsets between lung and peripheral blood (Fig. 4c), suggesting that expansions of these distinct adaptive-like NK cell subsets are independent from each other. We next analyzed the phenotype of CD49a^{+}KIR^{+}NKG2C^{+}CD56^{bright}CD16^{-} blood NK cells and found intermediate

224 expression of CD57 with relatively low co-expression of NKG2A (Fig. 4d, e).
225 Furthermore, CD49a^{+}KIR^{+}NKG2C^{+}CD56^{bright}CD16^{-} blood NK cells differed from
226 their counterpart in lung by low expression of both CD69 and CD103 (Fig. 4e, d).
227 Taken together, these results demonstrate the presence of a novel
228 CD49a^{+}KIR^{+}NKG2C^{+}CD16^{-} NK cell subset in the peripheral blood of a subset of
229 donors emerging independently from adaptive-like CD56^{dim}CD16^{+} NK cells.
230
231 *Peripheral blood CD49a^{+}KIR^{+}NKG2C^{+}CD56^{bright}CD16^{-} NK cells share features with*
232 *lung trNK cells and adaptive-like NK cells*
233 The presence of adaptive-like lung trNK cells in patients undergoing surgery
234 for suspected lung cancer did not significantly correlate with any demographical or
235 clinical parameters including age, gender, cigarette smoking, COPD, the type of lung
236 tumor, survival, lung function, or HCMV IgG concentrations in plasma (Supplementary
237 Fig. 2a-f). Therefore, we next assessed whether CD49a^{+}KIR^{+}NKG2C^{+}CD56^{bright}CD16^{-}
238 NK cells could also be identified in the blood of unrelated healthy blood donors. Indeed,
239 we found KIR^{+}NKG2C^{+} NK cells co-expressing CD49a in the CD56^{bright}CD16^{-} NK
240 cell subset in 16% of the blood donors (Fig. 5a, b). Within the CD56^{bright}CD16^{-} NK cell
241 subset, KIR^{+}NKG2C^{+} NK cells were almost exclusively detected in the CD49a^{+}
242 population (Fig. 5c), suggesting that this subset is a population distinct from activated
243 NK cells that have lost expression of CD16. Hence, we next sought to determine the
244 phenotypic profile of healthy blood CD49a^{+}KIR^{+}NKG2C^{+}CD56^{bright}CD16^{-} NK cells.
245 UMAP analysis of CD56^{bright}CD16^{-} NK cells from donors with CD49a^{+} NK cells in the
246 blood revealed a strong separation of the CD49a^{+} NK cell subset co-expressing KIR
247 and NKG2C based on lower expression or lack of CD69, CD45RA, CD57, CD38,
248 NKp80, and TIM-3 as well as high expression of CD8, CXCR3 and granzyme B on

249 CD49a^{+}KIR^{+}NKG2C^{+} NK cells (Fig. 5d). This phenotype could be confirmed in
250 individual samples (Fig. 5e). Interestingly, strong expression of CXCR6 could be
251 identified on CD69^{+}, but not on CD49a^{+}KIR^{+}NKG2C^{+}CD56^{bright}CD16^{-} NK cells,
252 indicating that this NK cell subset depends on other chemokine receptors such as
253 CXCR3 for tissue homing.

254 To gain further insight into the blood CD49a^{+}KIR^{+}CD56^{bright}CD16^{-} NK cells,
255 we sorted this subset and compared it to sorted blood CD49a^{-}KIR^{-}CD56^{bright}CD16^{-} NK
256 cells using RNAseq (Fig. 6a, see Supplementary Fig. 1c for gating strategy). We next
257 investigated whether gene expression differences in CD49a^{+}KIR^{+}CD56^{bright}CD16^{-} NK
258 cells indicated a different functional profile. Blood CD49a^{+}KIR^{+}CD56^{bright}CD16^{-} NK
259 cells expressed particularly higher levels of *CCL5*, *LAMP1, GZMH* and *GNLY*, and
260 lower levels of *XCL1*, *HIF1A*, *IL2RB*, and I*L18RAP* (Fig. 5f). Therefore, blood
261 CD49a^{+}KIR^{+}NKG2C^{+}CD56^{bright}CD16^{-} NK cells and adaptive-like lung trNK cells
262 (Fig. 3a) shared a common gene expression pattern for *CCL5*, *GZMH*, *IL2RB* and
263 *IL18RAP*, indicating that they are functionally distinct from their non-adaptive
264 counterparts.

265 To assess whether CD49a^{+}KIR^{+}CD56^{bright}CD16^{-} blood NK cells segregate
266 further at the transcriptome level, we analyzed differentially expressed genes between
267 CD49a^{+}KIR^{+}CD56^{bright}CD16^{-} NK cells and CD49a^{-}KIR^{-}CD56^{bright}CD16^{-} NK cells. A
268 total of 351 genes were differentially expressed (padj<0.01, log2FC>1) and clearly
269 segregated both subsets (Fig. 6a). Based on high protein expression of CD49a, pan-
270 KIR, NKG2C, CD8, and lower expression of NKp80 and CD45RA (Fig. 1e, f and Fig.
271 5d, e), CD49a^{+}KIR^{+}CD56^{bright}CD16^{-} blood NK resembled cells to some extent
272 adaptive-like trNK cells in the lung. In order to identify similarities also at
273 transcriptome level, we next compared genes that were differentially expressed in

274 CD49a^{+}KIR^{+}CD56^{bright}CD16^{-} compared to CD49a^{-}KIR^{-}CD56^{bright}CD16^{-} NK cells in
275 peripheral blood with genes that were differentially expressed between non-adaptive
276 trNK cells (defined as CD69^{+}CD49a^{+}CD103^{+}NKG2A^{+}NKG2C^{-}CD16^{-} NK cells) and
277 non-tissue-resident CD69^{-}CD56^{bright}CD16^{-} NK cells in lung (Fig. 6b).
278 CD49a^{+}KIR^{+}CD56^{bright}CD16^{-} blood NK cells shared 73 DEGs with non-adaptive trNK
279 cells in lung, including high expression of *ITGA1* (CD49a), *ZNF683* (Hobit), *PRDM1*
280 (Blimp-1), *CCL5*, *PIK3R1*, *PLA2G16*, *ATXN1*, as well as lower expression of *SELL*
281 (CD62L), *GPR183*, *IL18R1*, *IL18RAP*, *SOX4*, *RAMP1*, and *IFITM3* (Fig. 6b). All of
282 these genes have also been shown to be differentially expressed in trNK cells in the
283 bone marrow and/or CD8^{+} T_{RM} cells in lung[35,36]. It should however be noted that other
284 core-genes associated with tissue-resident lymphocytes (e.g. *S1PR1*, *S1PR5*, *CXCR6*,
285 *ITGAE*, *RGS1*, *KLF2*, *KLF3*, and *RIPOR2*) were not differentially expressed between
286 CD49a^{+}KIR^{+}CD56^{bright}CD16^{-} and CD49a^{-}KIR^{-}CD56^{bright}CD16^{-}NK cells, indicating
287 that they only partially have a tissue-resident phenotype.

288 In addition to differentially expressing genes associated with tissue-residency,
289 CD49a^{+}KIR^{+}CD56^{bright}CD16^{-} blood NK cells shared differentially expressed genes
290 with adaptive-like trNK cells in lung (Fig. 6c) and/or adaptive CD56^{dim}CD16^{+} NK cells
291 in peripheral blood[8,29], including increased expression of *KIRs*, *KLRC2*, *GZMH*,
292 *ITGAD*, *CCL5*, *IL32*, *ZBTB38*, *CD3E*, *ARID5B*, *MCOLN2*, and *CD52,* and decreased
293 expression of *KLRB1*, *FCER1G*, *IL18RAP*, *IL2RB2*, *TLE1*, *AREG*, and *KLRF1* (Fig.
294 6a, c, Supplementary Fig. 3).

295 Taken together, CD49a^{+}KIR^{+}CD56^{bright}CD16^{-} NK cells in the blood share traits
296 with both non-adaptive lung trNK cells, adaptive-like lung trNK cells, and adaptive-
297 like CD56^{dim} blood NK cells.

298

Increased metabolic modifications in adaptive-like CD49a^{+}NKG2C^{+}CD56^{bright}CD16^{-} blood and lung NK cells

Next, we sought to identify whether differential gene expression in CD49a^{+}NKG2C^{+}CD56^{bright}CD16^{-} NK cells is consistent with distinct pathways specific for this adaptive-like lung NK cell subset. Indeed, hallmark gene set enrichment analysis (GSEA) of CD49a^{+}NKG2C^{+}CD56^{bright}CD16^{-} blood NK cells revealed a strong enrichment for pathways associated with cell cycle arrest and DNA repair, including 'G2M checkpoint pathway', 'E2F targets', 'bile acid metabolism', 'UV response', and, although not significant, the 'reactive oxygen species (ROS) pathway' (Fig. 6d, Supplementary Fig. 4a). In adaptive-like lung trNK cells, only the ROS pathway was significantly enriched, with five of the relevant core genes identical both in blood and lung adaptive-like NK cells (i.e. *SOD1*, *SOD2*, *FTL*, *TXN* and *NDUFB4*) (Fig. 6e). Most significantly downregulated gene set pathways in adaptive-like CD49a^{+}NKG2C^{+}CD56^{bright}CD16^{-} NK cells were shared between peripheral blood and lung, including pathways involved in 'IL6 JAK STAT3 signaling', 'TNFA signaling via NFKB', 'IL2 STAT5 signaling', 'TGF beta signaling' and 'inflammatory response' (Fig. 6f, g, Supplementary Fig. 4b, c). In addition to the above-mentioned pathways involved in metabolic modifications, several distinct genes have been shown to be associated to oxidative stress in cytokine-stimulated CD8^{+} T and NK cells[37-39]. Indeed, gene expression levels for *TXN1*, *PRDX1*, and *SOD1* were higher in CD49a^{+}KIR^{+}NKG2C^{+} CD56^{bright}CD16^{-} NK cells in both peripheral blood and lung as compared to the non-adaptive counterpart (Supplementary Fig. 4d). However, while *DUSP1* and *TXNIP*[39] were downregulated in adaptive-like lung trNK cells (Supplementary Fig. 4e), no changes were observed in adaptive-like CD49a^{+}CD56^{bright}CD16^{-} NK cells in healthy blood (Supplementary Fig. 4e).

Together, these results indicate modifications in the cellular metabolism in adaptive-like CD49a^{+}KIR^{+}NKG2C^{+}CD56^{bright}CD16^{-} NK cells in blood and lung, potentially caused by cytokine-induced stimulation and/or mitophagy during the contraction-to-memory transition as discussed previously for murine memory NK cells[40] and antigen-specific CD8^{+} T cells[41], respectively.

Discussion

Distinct subsets of putative human adaptive-like NK cells have been described within the CD56^{dim}CD16^{+} subset in peripheral blood[5,6,8,10,42] and the CD56^{bright}CD16^{-} subset in liver[7]. Here, we identified and characterized a yet unexplored and unique subset of adaptive-like KIR^{+}NKG2C^{+}CD56^{bright}CD16^{-} NK cells in the human lung and healthy human blood (Fig. 7). The lung adaptive-like NK cells displayed a tissue-residency phenotype as indicated by co-expression of CD69, CD49a and CD103. Lung adaptive-like trNK cells shared several phenotypic features with other adaptive-like NK cell subsets both in blood and/or liver, including high expression of CD49a (liver), CD69 (liver), CD2 (blood) and lack or lower expression of CD57 (liver), CD45RA (liver) and perforin (liver), as well as low expression of FcεR1γ and Siglec-7 (blood)[5,7-10,24,42,43]. However, lung adaptive-like NK cells segregate from their counterpart in the liver by high expression of Eomes and CD103 and from those in blood by lack of CD57 and a CD56^{bright}CD16^{-} phenotype. Transcriptome analysis revealed shared core genes in lung adaptive-like trNK cells and blood CD56^{dim}CD16^{+} adaptive-like NK cells, underlining common features between the two subsets. Intriguingly, lung adaptive-like trNK cells were highly target cell-responsive, and the overall blood and lung NK cell populations were hyperresponsive in donors with expansions of adaptive-like trNK cells in the lung. These findings indicate *in vivo* priming, which, however, did not correlate with presence of tumor, HCMV serostatus, infection, or clinical and demographic parameters. In fact, we could identify CD49a^{+}KIR^{+}NKG2C^{+}CD56^{bright}CD16^{-} NK cells also in the peripheral blood of healthy donors. These cells shared core gene sets with adaptive-like NK cells subsets both in blood and lung and, despite the lack of CD103, also with non-adaptive trNK cells, indicating tissue imprinting. Recently, a minute subset of T_{EM} cells expressing a tissue

signature has been shown in peripheral blood[44]. These findings suggest re-entry of tissue-resident memory-associated lymphocytes from tissue into circulation. However, it is yet unknown whether precursors of conventional or adaptive-like human lung trNK cells are seeding the tissue from the circulation or whether the pool of trNK cells is mainly replenished by proliferation within the tissue. In mice, MCMV-specific $CD8^+$ T cells convert to $CD103^+$ T_{RM} cells, with small numbers of new T_{RM} cells deriving from the circulation[45], and memory inflation is required for retention of $CD8^+$ T_{RM} cells in the lungs after intranasal vaccination with MCMV[46]. This indicates a dynamic retention of T_{RM} cells by a persistent infection. In self-limiting viral infections of the respiratory tract, conventional epitopes induce $CD8^+$ T_{RM} cells that wane over time[47]. It remains to be determined whether virus-dependent expansion and maintenance of T_{RM} cells is analogous in adaptive-like trNK cells in the lung. Our data indicate, however, that T_{RM} cells and adaptive-like NK cells differ in their recruitment to the lung, with T_{RM} cells being dependent on CXCR6[48] while $CD49a^+KIR^+NKG2C^+CD56^{bright}CD16^-$ blood NK cells lacked CXCR6 but expressed high levels of CXCR3.

Since we showed that adaptive-like lung trNK cells were hyperresponsive, they might be clinically relevant, e.g. in the defense against malignant target cells. Lung $CD8^+$ T_{RM} cells have previously been shown to be able to control tumor growth and to be essential for anti-cancer vaccination in mice and also correlated with increased survival in lung cancer patients[49]. In addition to strong target cell-responsiveness, we observed increased gene expression levels of *GZMH* and *CCL5* in adaptive-like lung and blood NK cells, respectively. An antiviral activity has been proposed for granzyme H[50,51], however, a direct association of this effector molecule with adaptive-like NK cells remains to be determined. CCL5 and XCL1, chemokines upregulated in adaptive-

like lung trNK cells, were predominantly produced by mouse Ly49H$^+$ NK cells upon stimulation with MCMV-derived m157 protein[52], and CCL5 has been shown to be specifically expressed by CD8$^+$ memory T_{EM} cells[53]. Thus, adaptive-like CD49a$^+$KIR$^+$NKG2C$^+$CD56^{bright}CD16$^-$ blood and lung NK cells share also functional characteristics with other memory lymphocyte subsets.

Adaptive-like lung trNK cell expansions were rarely observed in donors with adaptive-like CD56^{dim}CD16$^+$ NK cell expansions, indicating that these two distinct subsets have distinct developmental cues. Indeed, even in the rare cases where we could detect expansions of both adaptive-like lung trNK cells and CD56^{dim}CD16$^+$ NK cells in the same individual, these populations displayed distinct KIR repertoires. Furthermore, expansions of adaptive-like lung trNK cells were detected in HCMV-seronegative individuals (Supplementary Fig. 2e, f), while expansions of adaptive-like CD56^{dim}CD16$^+$ NK cells were restricted to HCMV-seropositive individuals (Supplementary Fig. 2e)[5,42]. It thus remains possible that other viral infections could drive the expansion of adaptive-like trNK cells, as has previously been suggested for the generation of cytokine-induced memory NK cells after influenza virus infection in humans[54] and mice[15]. Taken together, our data support a model where adaptive-like trNK cells and adaptive-like CD56^{dim}CD16$^+$ NK cells develop independently from each other, possibly due to distinct environmental requirements for their expansion.

Our results revealed accumulation of gene sets predictive of adaptive-like lung trNK cells controlling dysfunctional mitochondria and ROS. In mice, MCMV-specific Ly49H$^+$ NK cells have been shown to control the removal of dysfunctional mitochondria via mitophagy, allowing the formation of a stable reservoir of memory NK cells[40]. Human adaptive-like CD56^{dim}CD16$^+$ NK cells displayed an elevated mitochondrial function and quality[29], and mitochondrial fitness was crucial for the

404 generation of $CD8^+$ T cell memory[55]. Hence, metabolic adaptations might be a common
405 characteristic between different lines of adaptive-like cytotoxic lymphocytes.
406 Together, our data reveal the presence of a yet unexplored and distinct adaptive-
407 like trNK cell subset in the human lung, indicating that adaptive-like NK cells are not
408 confined to peripheral blood and/or liver. Expansions of adaptive-like trNK cells in the
409 lung are mostly accompanied by the presence of
410 $CD49a^+KIR^+NKG2C^+CD56^{bright}CD16^-$ NK cells in peripheral blood, enabling the non-
411 invasive identification of potential donors with adaptive-like lung trNK cell expansions.
412 Since adaptive-like trNK cells were strongly target cell-responsive, these cells might
413 be clinically relevant in the defense of lung cancer and/or respiratory viral infections.

Material and methods

Lung patients and healthy blood

A total of 103 patients undergoing lobectomy for suspected lung cancer were included in this study. None of the patients received preoperative chemotherapy and/or radiotherapy. Patients with records of strong immunosuppressive medication and/or hematological malignancy were excluded from the study. Clinical and demographic details are summarized in Table 1. Furthermore, healthy blood was collected from regular blood donors. The regional review board in Stockholm approved the study, and all donors gave informed written consent prior to collection of samples.

Processing of tissue specimens and peripheral blood

Lung tissue was processed as previously described[20]. Briefly, a small part of macroscopically tumor-free human lung tissue from each patient was transferred into ice-cold Krebs-Henseleit buffer and stored on ice for less than 18 h until further processing. The tissue was digested using collagenase II (0.25 mg/ml, Sigma-Aldrich) and DNase (0.2 mg/ml, Roche), filtered and washed in complete RPMI 1640 medium (Thermo Scientific) supplemented with 10% FCS (Thermo Scientific), 1 mM L-glutamine (Invitrogen), 100 U/ml penicillin, and 50 µg/ml streptomycin (R10 medium). Finally, mononuclear cells from the lung cell suspensions and peripheral blood were isolated by density gradient centrifugation (Lymphoprep).

RNA-sequencing and RNAseq data analysis

RNA of sorted NK cell subsets from blood and lung were sequenced and analyzed as described previously[25]. Briefly, RNAseq was performed using a modified version of

the SMART-Seq2 protocol[56]. For analysis of lung adaptive-like NK cells, live NKG2C$^+$KIR$^+$CD3$^-$CD14$^-$CD19$^-$CD56$^+$CD16$^-$ NK cells were sorted from two donors and were compared to previously published data on CD69$^+$CD49a$^+$CD103$^-$ and CD69$^+$CD49a$^+$CD103$^+$ NKG2A$^+$CD16$^-$ trNK cells (GSE130379)[25]. For analysis of KIR$^+$CD49a$^+$ CD56^{bright}CD16$^-$ NK cells, we sorted KIR$^+$CD49a$^+$ and KIR$^-$CD49a$^-$ live CD14$^-$CD19$^-$CD3$^-$CD56^{bright}CD16$^-$ NK cells from cryopreserved PBMCs from 4 donors. Duplicates of 100 cells from each population from two individual donors were sorted into 4.2ul of lysis buffer (0.2% Triton X-100, 2.5uM oligo-dT (5′-AAGCAGTGGTATCAACGCAGAGTACT30VN-3′), 2.5mM dNTP, RNAse Inhibitor (Takara), and ERCC RNA spike in controls (Ambion)) in a 96-well V-bottom PCR plate (Thermo Fisher). Sorted cells were then frozen and stored at -80°C until they could be processed. Subsequent steps were performed following the standard SMART-Seq2 protocol with 22 cycles of cDNA amplification and sample quality was determined using a bioanalyzer (Agilent, High Sensitivity DNA chip). 5ng of amplified cDNA was taken for tagmentation using a customized in-house protocol[57] and Nextera XT primers. Pooled samples were sequenced on a HiSeq2500 on high output mode with paired 2x125bp reads.

Transcriptome analysis

Following sequencing and demultiplexing, read pairs were trimmed from Illumina adapters using cutadapt (version 1.14)[58], and UrQt was used to trim all bases with a phred quality score below 20[59]. Read pairs were subsequently aligned to the protein coding sequences of the human transcriptome (gencode.v26.pc_transcripts.fa) using Salmon (version 0.8.2)[60], and gene annotation using gencode.v26.annotation.gtf. DeSeq2[61] was used to analyze RNA-seq data in R studio version 1.20. Briefly, raw

count values were used as input into deSeq2, and variance stabilizing transformation was used to transform data. Data were batch- and patient corrected using Limma[62]. A cut-off of >100 counts across the samples was used to filter out low expressed genes. Genes with an adjusted p-value<0.05 and a log2-fold change greater than 1 were considered as differentially expressed between paired samples. Similarly, previously published data sets on adaptive-like NKG2C^{+}CD57^{+}CD56^{dim}CD16^{+} NK cells and conventional NKG2C^{-}CD57^{+}CD56^{dim} NK cells (GSE117614)[29] were analyzed using deSeq2 to identify differentially expressed genes. Heatmaps of gene expression were generated using Pheatmap in R and show the z-score for differentially expressed genes (as determined above in deSeq2) for all donors and replicates.

Flow cytometry

Antibodies and clones reactive against the following proteins were used: CD2 (TS1/8, BV421 or Pacific Blue, Biolegend), CD3 (UCHT1, PE-Cy5, Beckman Coulter), CD8 (RPA-T8, Brilliant Violet 570, Biolegend, or RPA-8, BUV395 or SK1, BUV737, BD Biosciences), CD14 (MφP9, Horizon V500, BD Biosciences), CD16 (3G8, Brilliant Violet 570 or Brilliant Violet 711, or Brilliant Violet 785, Biolegend), CD19 (HIB19, Horizon V500, BD Biosciences), CD38 (HIT2, Brilliant Violet 711 or BUV661, BD Biosciences), CD45 (HI30, Alexa Fluor 700, Biolegend, or BUV805, BD Biosciences), CD45RA (HI100, Brilliant Violet 785, Biolegend), CD49a (TS2A, AlexaFluor 647, Biolegend, or HI30, BUV615, or 8R84, Brilliant Violet 421, BD Biosciences), CD56 (N901, ECD, Beckman Coulter, or HCD56, Brilliant Violet 711, Biolegend, or NCAM16.2, PE-Cy7, or BUV563, BD Biosciences), CD57 (TB01, purified, eBioscience, or HNK-1, Brilliant Violet 605, Biolegend), CD103 (APC, B-Ly7, eBioscience, or biotin, 2G5, Beckman Coulter, or Ber-ACT8, Brilliant Violet 711,

BUV395, BD Biosciences, or Ber-ACT8, PE-Cy-7, Biolegend), KIR2DL1 (FAB1844F, biotin, R&D Systems), KIR2DL3 (180701, FITC, R&D Systems), KIR3DL1 (DX9, Brilliant Violet 421, Biolegend), KIR3DL2 (DX-31, Brilliant Violet 711, Biolegend), KIR2DL2/S2/L3 (GL183, PE-Cy5.5, Beckman Coulter), KIR2DL1/S1 (EB6, PE-Cy5.5 or PE-Cy7, Beckman Coulter), NKG2A (Z1991.10, APC-A780, or PE, Beckman Coulter, or 131411, BUV395, BD Biosciences), NKG2C (134591, Alexa-Fluor 488 or PE, R&D Systems), CD69 (TP1.55.3, ECD, Beckman Coulter, or FN50, PE-CF594, BD Biosciences, or FN50, Brilliant Violet 786, Biolegend), CD127 (Brilliant Violet 421, HIL-7R-M21, BD Biosciences or PE-Cy7, R34.34, Beckman Coulter), CD161 (HP3-3G10, Brilliant Violet 605 or APC/Fire 750, Biolegend), CXCR3 (Alexa Fluor 647, G025H7, Biolegend), CXCR6 (K041E5, Brilliant Violet 421, Biolegend), CD85j/ILT2 (HP-F1, Super Bright 436, Invitrogen), NKp80 (5D12, PE, BD Biosciences, or 4A4.D10, PE-Vio770, Miltenyi), Siglec-7 (5-386, Alexa Fluor 488, Bio-Rad), TIM-3 (7D3, Brilliant Violet 711, BD Biosciences). After two washes, cells were stained with streptavidin Qdot 605 or Qdot 585 (both Invitrogen), anti-mouse IgM (II/41, eFluor 650NC, eBioscience) and Live/Dead Aqua (Invitrogen). After surface staining, peripheral blood mononuclear cells (PBMC) were fixed and permeabilized using FoxP3/Transcription Factor staining kit (eBioscience). For intracellular staining the following antibodies were used: Eomes (WF1928, FITC, eBioscience), FcεR1γ (polyclonal, FITC, Merck), granzyme B (GB11, BB790, BD Biosciences), Ki67 (B56, Alexa Fluor 700, BD Biosciences), perforin (dG9, BB755, BD Biosciences, or B-D48, Brilliant Violet 421, Biolegend), T-bet (4B10, Brilliant Violet 421, BD Biosciences), and TNF (MAb11, Brilliant Violet 421, Biolegend, or Brilliant Violet 650, BD Biosciences). Purified NKG2C (134591, R&D Systems) was

biotinylated using a Fluoreporter Mini-biotin XX protein labeling kit (Life Technologies) and detected using streptavidin-Qdot 585, 605 or 655 (Invitrogen).

Samples were analyzed on a BD LSR Fortessa equipped with four lasers (BD Biosciences) or a BD FACSymphony A5 equipped with five lasers (BD Biosciences), and data were analyzed using FlowJo version 9.5.2 and version 10.6.1 (Tree Star Inc). UMAPs were constructed in FlowJo 10.6.1 using the UMAP plugin. UMAP coordinates and protein expression data were subsequently exported from FlowJo, and protein expression for each parameter was normalized to a value between 0 and 100. UMAP plots were made in R using ggplot, and color scale show log2(normalized protein expression +1).

For sorting of NK cells from lung and peripheral blood for RNA sequencing, thawed cryopreserved mononuclear cells were stained with anti-human CD57 (NK-1, FITC, BD Biosciences), CD16 (3G2, Pacific Blue, BD Biosciences), CD14 (MφP9, Horizon V500, BD Biosciences), CD19 (HIB19, Horizon V500, BD Biosciences), CD103 (Ber-ACT8, Brilliant Violet 711, BD Biosciences), CD49a (TS2/7, Alexa Fluor 647, Biolegend), CD45 (HI30, A700, Biolegend), CD8 (RPA-T8, APC/Cy7, BD Biosciences), NKG2A (Z199.10, PE, Beckman Coulter), CD69 (TP1.55.3, ECD, Beckman Coulter), CD3 (UCHT1, PE/Cy5, Beckman Coulter), KIR2DL1/S1 (EB6, PE/Cy5.5, Beckman Coulter), KIR2DL2/3/S2 (GL183, PE/Cy5.5, Beckman Coulter,), NKG2C (134591, biotin, R&D Systems, custom conjugate), CD56 (NCAM16.1, PE/Cy7, BD Biosciences), streptavidin Qdot655 (Invitrogen), and Live/Dead Aqua (Invitrogen).

DNA isolation and KIR/HLA-ligand genotyping

Genomic DNA was isolated using a DNeasy Blood & Tissue Kit (Qiagen) from 100 µl of whole blood. KIR genotyping and KIR ligand-determination were performed using PCR-SSP technology with a *KIR* typing kit and a *KIR HLA* ligand kit (both Olerup-SSP) according to the manufacturer's instructions.

CMV IgG ELISA

Concentrations of anti-CMV IgG relative to a standard curve and internal negative and positive control were determined by ELISA (Abcam, UK) and read in a microplate spectrophotometer (Bio-Rad xMark) at 450nm with a 620nm reference wavelength.

Activation assay

Degranulation and TNF production of fresh blood and lung NK cells were assessed as previously described[20,22]. In brief, fresh lung and blood mononuclear cells were resuspended in R10 medium and rested for 15 to 18 hours at 37°C. Subsequently, the cells were co-cultured in R10 medium alone or in presence of K562 cells for 2 hours in the presence of anti-human CD107a (FITC or Brilliant Violet 421, H4A3, BD Biosciences, San Jose, Calif.).

Statistics

GraphPad Prism 6 and 7 (GraphPad Software) was used for statistical analysis. For each analysis, measurements were taken from distinct samples. The statistical method used is indicated in each figure legend.

Data Availability

The dataset generated for this study can be found in the Gene Expression Omnibus with accession no. xxxx (data will be deposited and made available before publication).

Author contribution

Conceptualization: N.M., H.G.L., Ja.M.; Methodology: N.M., Ja.M.; Investigation: N.M., M.S., Je.M., J.H., E.K., M.B., S.N., J.N.W.; Resources: M.A.-A.; Writing – original draft: N.M., Ja.M.; Writing – review and editing: N.M., Ja.M., H.G.L; Visualization: N.M., Ja.M.; Funding acquisition: N.M., Ja.M., H.G.L.

Acknowledgements

The authors acknowledge support from the National Genomics Infrastructure in Stockholm funded by Science for Life Laboratory, the Knut and Alice Wallenberg Foundation, the Swedish Research Council, and SNIC/Uppsala Multidisciplinary Center for Advanced Computational Science for assistance with massively parallel sequencing and access to the UPPMAX computational infrastructure. The authors also acknowledge the MedH Core Flow Cytometry Facility (Karolinska Institutet), supported by Karolinska Institutet and Region Stockholm, for providing cell-sorting services. Furthermore, the authors want to thank all donors for participating in the study and A.-C. Orre, V. Jackson, and S. Hylander for administrative and clinical help as well as E. Yilmaz for assistance in the laboratory. This work was supported by the Swedish Research Council, the Strategic Research Foundation, the Swedish Foundation for Strategic Research, the Swedish Cancer Society, Sweden's Innovation Agency, the Eva and Oscar Ahréns Research Foundation, the Åke Wiberg Foundation and the Tornspiran Foundation.

584

585 **Disclosures**

586 The authors have no financial or other conflicts of interest.

Figure legends

Figure 1: Adaptive-like KIR^{+}NKG2C^{+} NK cells exist in the CD56^{bright}CD16^{-} NK cell subset in the human lung. (a) Representative overlay displaying pan-KIR and NKG2C expression on CD56^{dim}CD16^{+} NK cells in matched blood (black contour) and lung (orange). **(b)** Representative dot plots displaying pan-KIR and NKG2C expression on CD56^{bright}CD16^{-} NK cells in the lungs of three different donors. **(c)** Summary of data showing the frequencies of KIR^{+}NKG2C^{+} NK cells in CD56^{dim}CD16^{+} and CD56^{bright}CD16^{-} NK cells in blood and lung (n = 77). Friedman test, Dunn's multiple comparisons test. ***p<0.001, ****p<0.0001. **(d)** UMAP analysis of CD56^{bright}CD16^{-} lung NK cells from four donors with 2,000 events/donor (942 events in one of the donors). UMAPs were constructed using expression of Siglec-7, CD8, CD2, CD57, CD161, NKG2C, CD56, CD45RA, NKG2A and NKp80. Color scale shows log2(normalized expression + 1). **(e)** Representative histograms and **(f)** summary of data showing surface expression of NKG2A (n = 27), CD57 (n = 27), Siglec-7 (n = 7), CD161 (n = 12), CD2 (n = 5), ILT2 (n = 6), CD8 (n = 20), NKp80 (n = 6), CD45RA (n = 5), and intracellular expression of FcεR1γ (n = 4), Eomes (n = 7) and T-bet (n = 6) in KIR^{+}NKG2C^{+} NK cells in CD56^{dim}CD16^{+} blood (grey) and lung (orange) NK cells and CD56^{bright}CD16^{-} lung NK cells (blue). Friedman test, Dunn's multiple comparisons test. *p<0.05, **p<0.01, ***p<0.001, ****p<0.0001.

Figure 2: Adaptive-like CD56^{bright}CD16^{-} lung NK cells are tissue-resident. (a) Overlay of UMAPs from data from Figure 1, showing the position of NKG2C^{+} (blue) and NKG2C^{-} (grey) populations among CD56^{bright}CD16^{-} NK cells. **(b)** Expression of the tissue-residency markers CD69, CD49a, and CD103 within the UMAP of CD56^{bright}CD16^{-} lung NK cells. **(c)** Representative histograms and **(d)** summary of data

showing the expression of the tissue-residency markers CD69 (n = 23), CD49a (n= 21) and CD103 (n = 21) on $CD56^{dim}CD16^{+}$ blood (grey) and lung (orange) NK cells and $CD56^{bright}CD16^{-}$ lung NK cells (blue), respectively. Friedman test, Dunn's multiple comparisons test. *p<0.05, **p<0.01, ***p<0.001, ****p<0.0001. **(e)** Heatmap showing 102 differentially expressed genes between $KIR^{+}NKG2C^{+}$ trNK cells and $KIR^{-}NKG2C^{-}$ trNK cells in the human lung. Differentially expressed genes shared with $CD57^{+}NKG2C^{+}CD56^{dim}CD16^{+}$ adaptive-like NK cells in blood (from GSE117614) are highlighted in red. **(f)** Log2 fold-change for $NKG2C^{-}$ trNK cells vs $KIR^{+}NKG2C^{+}$ trNK cells in lung against log2 fold change for CD57+NKG2C- vs $CD57^{+}NKG2C^{+}$ $CD56^{dim}$ NK cells in blood. Data for $CD56^{dim}$ NK cells in peripheral blood are from GSE117614 [29]. **(g-i)** Single KIR expression analysis on $CD56^{dim}CD16^{+}$ NK cells from peripheral blood (red), $CD49a^{-}CD103^{-}CD56^{dim}CD16^{+}$ or $CD103^{-}CD56^{dim}CD16^{+}$ (black) and $CD49a^{+}CD103^{+}CD56^{bright}CD16^{-}$ or $CD103^{+}CD56^{bright}CD16^{-}$ (blue) NK cells in matched lung of three different donors. Educating KIR are highlighted in red. **(g)** Donor with expansions of self-KIR^{+} NK cells both in the $CD56^{dim}CD16^{+}$ subset in blood and lung and in the $CD56^{bright}CD16^{-}$ NK cell subset in the lung. **(h)** Donor with an expansion of self-KIR^{+} NK cells exclusively in the $CD56^{bright}CD16^{-}$ NK cell subset in the lung. **(i)** Donor with expansions of self-KIR^{+} NK cells both in the $CD56^{dim}CD16^{+}$ and $CD56^{bright}CD16^{-}$ subsets in blood and lung, respectively.

Figure 3: Adaptive-like lung trNK cells are highly functional. (a) Gene expression levels (counts per million reads) for selected genes associated with functional capacity are shown for $CD49a^{+}KIR^{-}NKG2C^{-}$ and $CD49a^{+}KIR^{+}NKG2C^{+}$ lung trNK cells (clear circles: $CD49a^{+}CD103^{-}$ NK cells, filled circles: $CD49a^{+}CD103^{+}$ NK cells). Mean ± SEM is shown. **(b)** Representative histograms and **(c)** summary of data displaying

637 expression of perforin and granzyme B (GzmB) (n = 4) in $CD56^{dim}CD16^{+}$ and in
638 $CD49a^{-}KIR^{-}NKG2C^{-}$ as well as $CD49a^{+}KIR^{+}NKG2C^{+}$ NK cells within the
639 $CD56^{bright}CD16^{-}$ NK cell subset, respectively, in human lung ex vivo. $CD14^{-}CD19^{-}$
640 $CD3^{-}CD45^{+}CD127^{+}CD161^{+}$ cells were gated as controls in (b). Friedman test, Dunn's
641 multiple comparisons test. *p<0.05. **(d)** Representative dot plots showing expression
642 of CD107a and CD49a on $KIR^{-}NKG2C^{-}$ and $KIR^{+}NKG2C^{+}$ NK cells in a donor without
643 (upper panel) and with (lower panel) expansion of $CD49a^{+}KIR^{+}NKG2C^{+}$ NK cells in
644 the lung (expression KIR and NKG2C are displayed in the left panel for each of the
645 two donors). **(e)** Summary of data showing the frequency of K562 target cell-induced
646 $CD107a^{+}$ (left) and TNF^{+} (right) NK cell subsets from donors with NK cell expansions
647 in the human lung. Responses by unstimulated controls were subtracted from
648 stimulated cells (n = 3). Mean ± SD is shown. **(f)** Representative dot plots showing
649 expression of CD107a and TNF vs CD103 on $CD49a^{+}KIR^{-}NKG2C^{-}$ (upper panel) or
650 $CD49a^{+}KIR^{+}NKG2C^{+}$ (lower panel) bulk NK cells in a donor with an expansion of
651 $CD49a^{+}KIR^{+}NKG2C^{+}$ NK cells in the lung. **(g, h)** Summary of data showing the
652 frequencies of **(g)** $CD107a^{+}$ and **(h)** TNF^{+} NK cells in blood NK cells and in subsets of
653 lung NK cells ($CD49a^{-}CD103^{-}$, expressing either CD49a or CD103, or
654 $CD49a^{+}CD103^{+}$) from donors without (left panels, n = 5 for CD107a, n= 3 for TNF) or
655 with (right panels, n = 4) expansions of $KIR^{+}NKG2C^{+}$ trNK cells in the lung. Responses
656 by unstimulated controls were subtracted from stimulated cells. (g, h) Violin plots with
657 quartiles and median are shown. Friedman test, Dunn's multiple comparisons test.
658 *p<0.05.
659

660 **Figure 4: Expansions of adaptive-like trNK cell in the lung indicate presence of**
661 **adaptive-like $CD49a^{+}KIR^{+}NKG2C^{+}$ NK cells in matched blood (a)** Representative

dot plots displaying expression of CD49a and NKG2C on NK cells in lung and matched peripheral blood. **(b)** Summary of data of frequencies of $CD49a^{+}KIR^{+}NKG2C^{+}$ NK cells of the $CD16^{-}$ NK cell subset and of $CD49a^{-}KIR^{+}NKG2C^{+}$ cells in the $CD16^{+}$ NK cell subset in lung and peripheral blood. Adaptive-like NK cell "expansions" were identified as outliers (filled circles) using the Robust regression and Outlier removal (ROUT) method (ROUT coefficent Q=1). Error bars show the median with interquartile range (n = 86). Median with interquartile range is shown. **(c)** Euler diagram indicating overlaps and relationships between $CD16^{-}CD49a^{+}KIR^{+}NKG2C^{+}$ and $CD16^{+}CD49a^{-}KIR^{+}NKG2C^{+}$ NK cell expansions in peripheral blood and lung. The number of individuals with overlaps between the subsets and compartments are indicated in the circles. **(d)** Representative overlays and **(e)** summary of data showing phenotypic differences between $CD49a^{+}KIR^{+}NKG2C^{+}$ (blue) and $CD49a^{-}KIR^{-}NKG2C^{-}$ (grey) NK cells within the $CD56^{bright}CD16^{-}$ NK cell subset in blood. (NKG2A, n=6; CD57, n=5; CD69, n=6; CD103, n=6; CD127, n=3; CD161, n=4). Violin plots with quartiles and median are shown.

Figure 5: Expansions of $CD49a^{+}KIR^{+}NKG2C^{+}$ $CD56^{bright}CD16^{-}$ NK cells in healthy blood donors. (a) Representative dot plot (left plot) and overlay (right plot) showing expression of KIR and NKG2C (left plot), and CD49a on $KIR^{+}NKG2C^{+}$ NK cells (blue) versus $KIR^{-}NKG2C^{-}$ NK cells (grey) (right plot) within $CD16^{-}$ blood NK cells of healthy blood donors. **(b)** Identification of expansions (filled circles) of $CD49a^{-}KIR^{+}NKG2C^{+}$ within the $CD56^{dim}CD16^{+}$ NK cell subset (21 outliers, 20%) and $CD49a^{+}KIR^{+}NKG2C^{+}$ cells within the $CD56^{bright}CD16^{-}$ NK cell subset (17 outliers, 16%) via the ROUT method (see also Figure 4e). Error bars show the median with interquartile range. (n=95). Median with interquartile range is shown. **(c)** Frequencies

of KIR^{+}NKG2C^{+} cells of CD49a^{-}CD16^{-} or CD49a^{+}CD16^{-} NK cells in healthy blood. The respective maternal population comprised at least 45 cells (n=13). Wilcoxon matched-pairs signed rank test. **p<0.005 **(d)** UMAPs based on CD56^{bright}CD16^{-} NK cells from three donors with KIR^{+}NKG2C^{+}CD56^{bright}CD16^{-} NK cells. UMAPs were constructed using expression of CXCR3, CD161, Ki67, NKG2C, CD103, TIGIT, perforin, granzyme B, NKG2A, CD16, CD56, CD49a, CD38, CD8, CXCR6, CD4, CD57, CD45RA, NKp80, CD69, GL183/EB6 (KIR), and CD127. Color scale indicates log2(normalized protein expression +1) for each parameter. **(e)** Summary of protein expression on CD49a^{+}KIR^{+}NKG2C^{+} NK cells from peripheral blood from healthy donors. (CD69, n=11; CD103, n=7; CD57, n=11; NKG2A, n=11; CD127, n=7; CD161, n=7; CD8, n=11; CD38, n=5; CD45RA, n=4; NKp80, n=5; TIM-3, n=5; CXCR3, n=4; CXCR6, n=5; Ki67, n=5; perforin, n=7; granzyme B, n=5). Violin plots with quartiles and median are shown. **(f)** Gene expression levels (counts per million reads) for selected genes associated with functional capacity are shown for CD49a^{-}KIR^{-} and CD49a^{+}KIR^{+} blood CD56^{bright}CD16^{-} NK cells. Mean ± SEM is shown.

Figure 6: CD49a^{+}KIR^{+}NKG2C^{+}CD56^{bright}CD16^{-} NK cells in healthy blood donors share traits with both trNK cells and with adaptive-like trNK cells. (a) Heatmap showing 138 differentially expressed genes (padj<0.001, log2FC>2) between CD56^{bright}CD16^{-}CD49a^{-}KIR^{-} and CD56^{bright}CD16^{-}CD49a^{+}KIR^{+} NK cells in peripheral blood from unrelated healthy donors (n=4). Genes shared with trNK cells in the lung were highlighted in dark blue, shared with adaptive-like trNK cells in bright blue, and genes shared with adaptive-like CD56^{dim}CD16^{+} NK cells in healthy blood in orange. **(b)** Log2 fold-change for trNK cells vs CD56^{bright}CD16^{-} NK cells in lung against log2 fold-change for CD49a^{+}KIR^{+}CD56^{bright}CD16^{-} vs CD49a^{-}KIR^{-}CD56^{bright}CD16^{-} NK

712 cells in blood. **(c)** Log2 fold-change for $KIR^{+}NKG2C^{+}$ trNK cells vs $NKG2C^{-}$ trNK
713 cells in lung against log2 fold-change for $CD49a^{+}KIR^{+}CD56^{bright}CD16^{-}$ vs $CD49a^{-}KIR^{-}$
714 $CD56^{bright}CD16^{-}$ NK cells in blood. **(d)** GSEA from (a) showing significantly enriched
715 gene sets of adaptive-like NK cells in healthy blood. **(e)** Hallmark GSEA enrichment
716 plots for 'reactive oxygen species pathway' for $CD49a^{+}KIR^{+}NKG2C^{+}$ adaptive-like
717 NK cells in lung (left) and blood (right). Shared genes between lung and blood
718 enrichment plots are highlighted. Core gene sets are marked in red, and negative rank
719 metric scores in blue. **(f, g)** GSEA from (a) showing significantly enriched gene sets of
720 non-adaptive trNK cells in **(f)** lung and **(g)** blood. **(d, f, g)** Pathways which were unique
721 and not shared with the respective reference population are highlighted in blue, and
722 gene sets significantly enriched at a nominal p value <1% are highlighted in red.
723
724 **Figure 7: Overview adaptive-like NK cell subsets that can be identified in human**
725 **lung and/or peripheral blood.** Both unique and shared characteristics at protein and
726 transcriptome between adaptive-like lung trNK cells,
727 $CD49a^{+}KIR^{+}NKG2C^{+}CD56^{bright}CD16^{-}$ blood NK cells, and adaptive-like
728 $CD56^{dim}CD16^{+}$ blood NK cells are shown.

729 Table 1. Clinical and demographic details of the 103 patients included in the study.

730

	Non-smoker (n = 16)	**Current smoker** (n = 25)	**Ex-smoker** (n = 62)
Female / male	8 / 8	14 / 11	41 / 21
Age (y), mean ± SD	67 ± 13.4	67 ± 8.0	69 ± 7.1
FEV1/FVC (% of predicted) mean ± SD	100 ± 10.3	88 ± 13.7*	93 ± 14.9#
Pathology	***% (n)***	***% (n)***	***% (n)***
Non-malignant	6 (1)	4 (1)	2 (1)
Adenocarcinoma	44 (7)	52 (13)	76 (47)
Large cell carcinoma	0 (0)	12 (3)	3 (2)
Squamous cell carcinoma	6 (1)	16 (4)	5 (3)
Metastasis	0 (0)	4 (1)	3 (2)
Carcinoid	31 (5)	8 (2)	6 (4)
Adenosquamous carcinoma	6 (1)	0 (0)	3 (2)
Other§	6 (1)	4 (1)	2 (1)
Medication	***% (n)***	***% (n)***	***% (n)***
Inhaled corticosteroids	19 (3)	0 (0)	2 (1)
Statins	38 (6)	28 (7)	31 (19)
Systemic immunosuppression	0 (0)	4 (1)	5 (3)
Beta-agonists or anti-cholinergics	0 (0)	12 (3)	13 (8)
Inhaled corticosteroid and long-acting beta-agonist combination	0 (0)	8 (2)	6 (4)
Diagnoses affecting lung function	***% (n)***	***% (n)***	***% (n)***
Asthma	19 (3)	0 (0)	5 (3)
COPD	0 (0)	32 (8)	10 (6)
Other lung parenchyme disease	6 (1)	0 (0)	2 (1)

731 * n = 24

732 # n = 59

733 § = uncertain histopathological diagnosis, data missing, combined small cell carcinoma

734

References

1. Sun, J. C., Beilke, J. N. & Lanier, L. L. Adaptive immune features of natural killer cells. *Nature* **457,** 557–561 (2009).
2. Cooper, M. A. *et al.* Cytokine-induced memory-like natural killer cells. *Proceedings of the National Academy of Sciences of the United States of America* **106,** 1915–1919 (2009).
3. O'Leary, J. G., Goodarzi, M., Drayton, D. L. & Andrian, von, U. H. T cell- and B cell-independent adaptive immunity mediated by natural killer cells. *Nature immunology* **7,** 507–516 (2006).
4. Paust, S. *et al.* Critical role for the chemokine receptor CXCR6 in NK cell-mediated antigen-specific memory of haptens and viruses. *Nature immunology* **11,** 1127–1135 (2010).
5. Guma, M. *et al.* Imprint of human cytomegalovirus infection on the NK cell receptor repertoire. *Blood* **104,** 3664–3671 (2004).
6. Lopez-Vergès, S. *et al.* Expansion of a unique CD57^{+}NKG2Chi natural killer cell subset during acute human cytomegalovirus infection. *Proceedings of the National Academy of Sciences of the United States of America* **108,** 14725–14732 (2011).
7. Marquardt, N. *et al.* Cutting Edge: Identification and Characterization of Human Intrahepatic CD49a+ NK Cells. *J. Immunol.* **194,** 2467–2471 (2015).
8. Schlums, H. *et al.* Cytomegalovirus infection drives adaptive epigenetic diversification of NK cells with altered signaling and effector function. *Immunity* **42,** 443–456 (2015).
9. Lee, J. *et al.* Epigenetic modification and antibody-dependent expansion of memory-like NK cells in human cytomegalovirus-infected individuals. *Immunity* **42,** 431–442 (2015).
10. Béziat, V. *et al.* NK cell responses to cytomegalovirus infection lead to stable imprints in the human KIR repertoire and involve activating KIRs. *Blood* **121,** 2678–2688 (2013).
11. Cerwenka, A. & Lanier, L. L. Natural killer cell memory in infection, inflammation and cancer. *Nature reviews. Immunology* **16,** 112–123 (2016).
12. Kuijpers, T. W. *et al.* Human NK cells can control CMV infection in the absence of T cells. *Blood* **112,** 914–915 (2008).
13. Orr, M., Murphy, W. & Lanier, L. 'Unlicensed' natural killer cells dominate the response to cytomegalovirus infection. *Nature immunology* **11,** 321–327 (2010).
14. Smith, H. R. C. *et al.* Recognition of a virus-encoded ligand by a natural killer cell activation receptor. *Proceedings of the National Academy of Sciences of the United States of America* **99,** 8826–8831 (2002).
15. Li, T. *et al.* Respiratory Influenza Virus Infection Induces Memory-like Liver NK Cells in Mice. *J. Immunol.* **198,** 1242–1252 (2017).
16. Dou, Y. *et al.* Influenza vaccine induces intracellular immune memory of human NK cells. *PLoS ONE* **10,** e0121258 (2015).
17. Gillard, G. O. *et al.* Thy1+ NK [corrected] cells from vaccinia virus-primed mice confer protection against vaccinia virus challenge in the absence of adaptive lymphocytes. *PLoS Pathog.* **7,** e1002141 (2011).
18. Reeves, R. K. *et al.* Antigen-specific NK cell memory in rhesus macaques. *Nature immunology* **16,** 927–932 (2015).

19. Gordon, C. L. *et al.* Tissue reservoirs of antiviral T cell immunity in persistent human CMV infection. *The Journal of experimental medicine* **214,** 651–667 (2017).
20. Marquardt, N. *et al.* Human Lung NK Cells are Predominantly Comprised of Highly Differentiated Hypofunctional CD69(-)CD56(dim) Cells. *J. Allergy Clin. Immunol.* **139,** 1321–1330.e4 (2016).
21. Cooper, G. E., Ostridge, K., Khakoo, S. I., Wilkinson, T. M. A. & Staples, K. J. Human CD49a+ Lung Natural Killer Cell Cytotoxicity in Response to Influenza A Virus. *Front Immunol* **9,** 1671 (2018).
22. Scharenberg, M. *et al.* Influenza A Virus Infection Induces Hyperresponsiveness in Human Lung Tissue-Resident and Peripheral Blood NK Cells. *Front Immunol* **10,** 1116 (2019).
23. Chiesa, Della, M. *et al.* Phenotypic and functional heterogeneity of human NK cells developing after umbilical cord blood transplantation: a role for human cytomegalovirus? *Blood* **119,** 399–410 (2012).
24. Liu, L. L. *et al.* Critical Role of CD2 Co-stimulation in Adaptive Natural Killer Cell Responses Revealed in NKG2C-Deficient Humans. *Cell Rep* **15,** 1088–1099 (2016).
25. Marquardt, N. *et al.* Unique transcriptional and protein-expression signature in human lung tissue-resident NK cells. *Nat Commun* **10,** 3841–12 (2019).
26. Emgård, J. *et al.* Oxysterol Sensing through the Receptor GPR183 Promotes the Lymphoid-Tissue-Inducing Function of Innate Lymphoid Cells and Colonic Inflammation. *Immunity* **48,** 120–132.e8 (2018).
27. Adams, N. M. *et al.* Transcription Factor IRF8 Orchestrates the Adaptive Natural Killer Cell Response. *Immunity* **48,** 1172–1182.e6 (2018).
28. Lau, C. M. *et al.* Epigenetic control of innate and adaptive immune memory. *Nature immunology* **19,** 963–972 (2018).
29. Cichocki, F. *et al.* ARID5B regulates metabolic programming in human adaptive NK cells. *The Journal of experimental medicine* **215,** 2379–2395 (2018).
30. Foley, B. *et al.* Cytomegalovirus reactivation after allogeneic transplantation promotes a lasting increase in educated NKG2C+ natural killer cells with potent function. *Blood* **119,** 2665–2674 (2012).
31. Ray, S. J. *et al.* The collagen binding alpha1beta1 integrin VLA-1 regulates CD8 T cell-mediated immune protection against heterologous influenza infection. *Immunity* **20,** 167–179 (2004).
32. Cheuk, S. *et al.* CD49a Expression Defines Tissue-Resident CD8(+) T Cells Poised for Cytotoxic Function in Human Skin. *Immunity* **46,** 287–300 (2017).
33. Vento-Tormo, R. *et al.* Single-cell reconstruction of the early maternal-fetal interface in humans. *Nature* **563,** 347–353 (2018).
34. Masopust, D. *et al.* Dynamic T cell migration program provides resident memory within intestinal epithelium. *The Journal of experimental medicine* **207,** 553–564 (2010).
35. Melsen, J. E. *et al.* Human Bone Marrow-Resident Natural Killer Cells Have a Unique Transcriptional Profile and Resemble Resident Memory CD8+ T Cells. *Front Immunol* **9,** 1829 (2018).
36. Kumar, B. V. *et al.* Human Tissue-Resident Memory T Cells Are Defined by Core Transcriptional and Functional Signatures in Lymphoid and Mucosal Sites. *Cell Rep* **20,** 2921–2934 (2017).

37. Kaur, N. *et al.* T cells expanded in presence of IL-15 exhibit increased antioxidant capacity and innate effector molecules. *Cytokine* **55,** 307–317 (2011).
38. Mimura, K. *et al.* Upregulation of thioredoxin-1 in activated human NK cells confers increased tolerance to oxidative stress. *Cancer Immunol. Immunother.* **66,** 605–613 (2017).
39. Levring, T. B. *et al.* Tumor necrosis factor induces rapid down-regulation of TXNIP in human T cells. *Sci Rep* **9,** 16725–13 (2019).
40. O'Sullivan, T. E., Johnson, L. R., Kang, H. H. & Sun, J. C. BNIP3- and BNIP3L-Mediated Mitophagy Promotes the Generation of Natural Killer Cell Memory. *Immunity* **43,** 331–342 (2015).
41. Grayson, J. M., Laniewski, N. G., Lanier, J. G. & Ahmed, R. Mitochondrial potential and reactive oxygen intermediates in antigen-specific CD8+ T cells during viral infection. *J. Immunol.* **170,** 4745–4751 (2003).
42. Béziat, V. *et al.* CMV drives clonal expansion of NKG2C+ NK cells expressing self-specific KIRs in chronic hepatitis patients. *Eur. J. Immunol.* **42,** 447–457 (2012).
43. Hammer, Q., Rückert, T. & Romagnani, C. Natural killer cell specificity for viral infections. *Nature immunology* **19,** 800–808 (2018).
44. Szabo, P. A. *et al.* Single-cell transcriptomics of human T cells reveals tissue and activation signatures in health and disease. *Nat Commun* **10,** 4706–16 (2019).
45. Smith, C. J., Caldeira-Dantas, S., Turula, H. & Snyder, C. M. Murine CMV Infection Induces the Continuous Production of Mucosal Resident T Cells. *Cell Rep* **13,** 1137–1148 (2015).
46. Morabito, K. M. *et al.* Memory Inflation Drives Tissue-Resident Memory CD8+ T Cell Maintenance in the Lung After Intranasal Vaccination With Murine Cytomegalovirus. *Front Immunol* **9,** 1861 (2018).
47. Wu, T. *et al.* Lung-resident memory CD8 T cells (TRM) are indispensable for optimal cross-protection against pulmonary virus infection. *J. Leukoc. Biol.* **95,** 215–224 (2014).
48. Takamura, S. *et al.* Interstitial-resident memory CD8+ T cells sustain frontline epithelial memory in the lung. *The Journal of experimental medicine* **159,** jem.20190557 (2019).
49. Nizard, M. *et al.* Induction of resident memory T cells enhances the efficacy of cancer vaccine. *Nat Commun* **8,** 15221 (2017).
50. Tang, H., Li, C., Wang, L., Zhang, H. & Fan, Z. Granzyme H of cytotoxic lymphocytes is required for clearance of the hepatitis B virus through cleavage of the hepatitis B virus X protein. *J. Immunol.* **188,** 824–831 (2012).
51. Andrade, F., Fellows, E., Jenne, D. E., Rosen, A. & Young, C. S. H. Granzyme H destroys the function of critical adenoviral proteins required for viral DNA replication and granzyme B inhibition. *EMBO J.* **26,** 2148–2157 (2007).
52. Dorner, B. G. *et al.* Coordinate expression of cytokines and chemokines by NK cells during murine cytomegalovirus infection. *J. Immunol.* **172,** 3119–3131 (2004).
53. Swanson, B. J., Murakami, M., Mitchell, T. C., Kappler, J. & Marrack, P. RANTES production by memory phenotype T cells is controlled by a posttranscriptional, TCR-dependent process. *Immunity* **17,** 605–615 (2002).

880 54. Goodier, M. R. *et al.* Influenza Vaccination Generates Cytokine-Induced
881 Memory-like NK Cells: Impact of Human Cytomegalovirus Infection. *J.*
882 *Immunol.* (2016). doi:10.4049/jimmunol.1502049
883 55. van der Windt, G. J. W. *et al.* Mitochondrial respiratory capacity is a critical
884 regulator of CD8+ T cell memory development. *Immunity* **36,** 68–78 (2012).
885 56. Picelli, S. *et al.* Full-length RNA-seq from single cells using Smart-seq2. *Nat*
886 *Protoc* **9,** 171–181 (2014).
887 57. Picelli, S. *et al.* Tn5 transposase and tagmentation procedures for massively
888 scaled sequencing projects. *Genome Res.* **24,** 2033–2040 (2014).
889 58. Martin, M. Cutadapt removes adapter sequences from high-throughput
890 sequencing reads. *EMBnet.journal* **17,** 10 (2011).
891 59. Modolo, L. & Lerat, E. UrQt: an efficient software for the Unsupervised
892 Quality trimming of NGS data. *BMC Bioinformatics* **16,** 175 (2015).
893 60. Patro, R., Duggal, G., Love, M. I., Irizarry, R. A. & Kingsford, C. Salmon
894 provides fast and bias-aware quantification of transcript expression. *Nature*
895 *Methods* **14,** 417–419 (2017).
896 61. Love, M. I., Huber, W. & Anders, S. Moderated estimation of fold change and
897 dispersion for RNA-seq data with DESeq2. *Genome Biol.* **15,** 550 (2014).
898 62. Weigt, S. S. *et al.* Gene Expression Profiling of Bronchoalveolar Lavage Cells
899 Preceding a Clinical Diagnosis of Chronic Lung Allograft Dysfunction. *PLoS*
900 *ONE* **12,** e0169894 (2017).
901

Figure 1

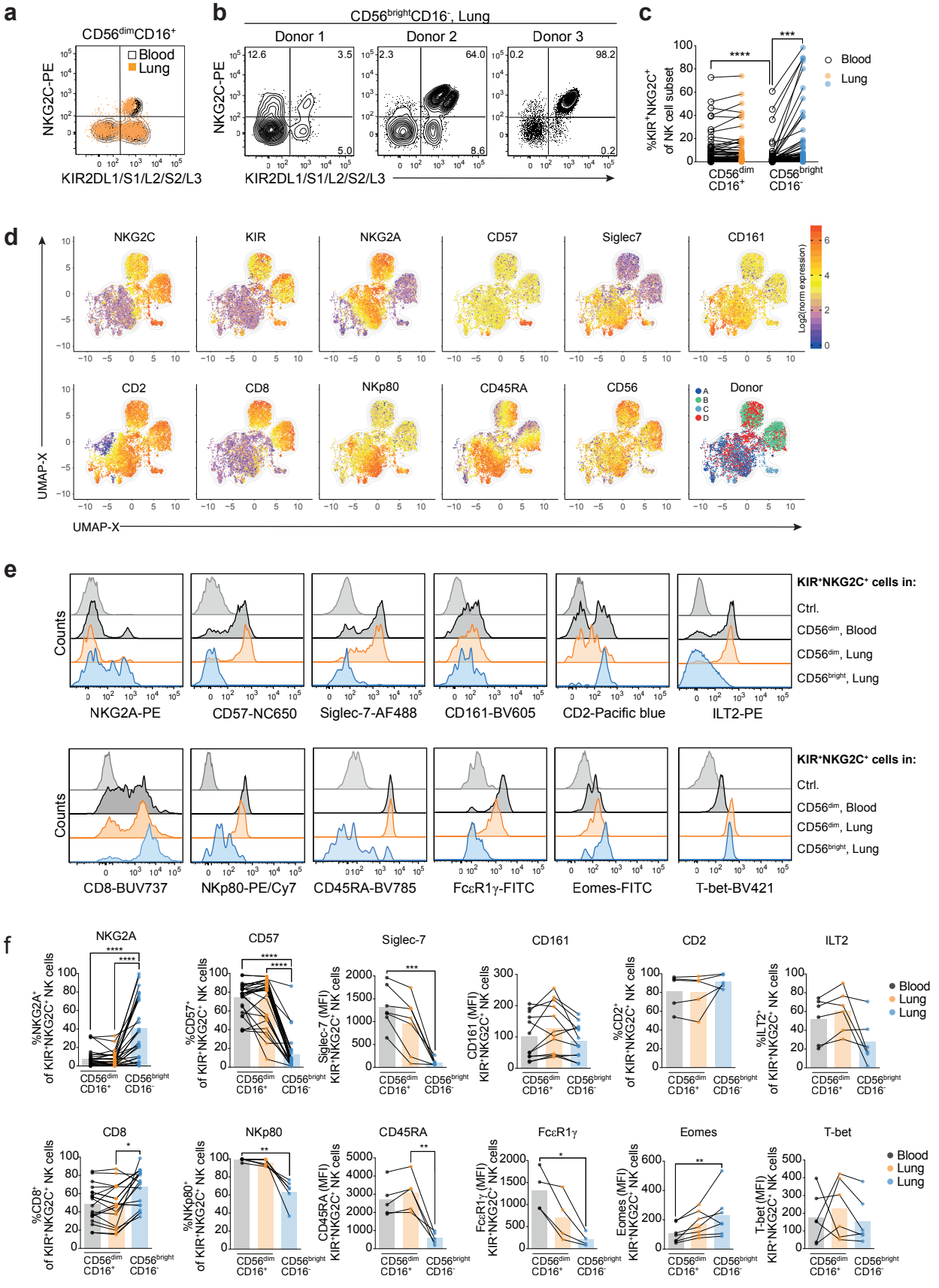

Figure 2

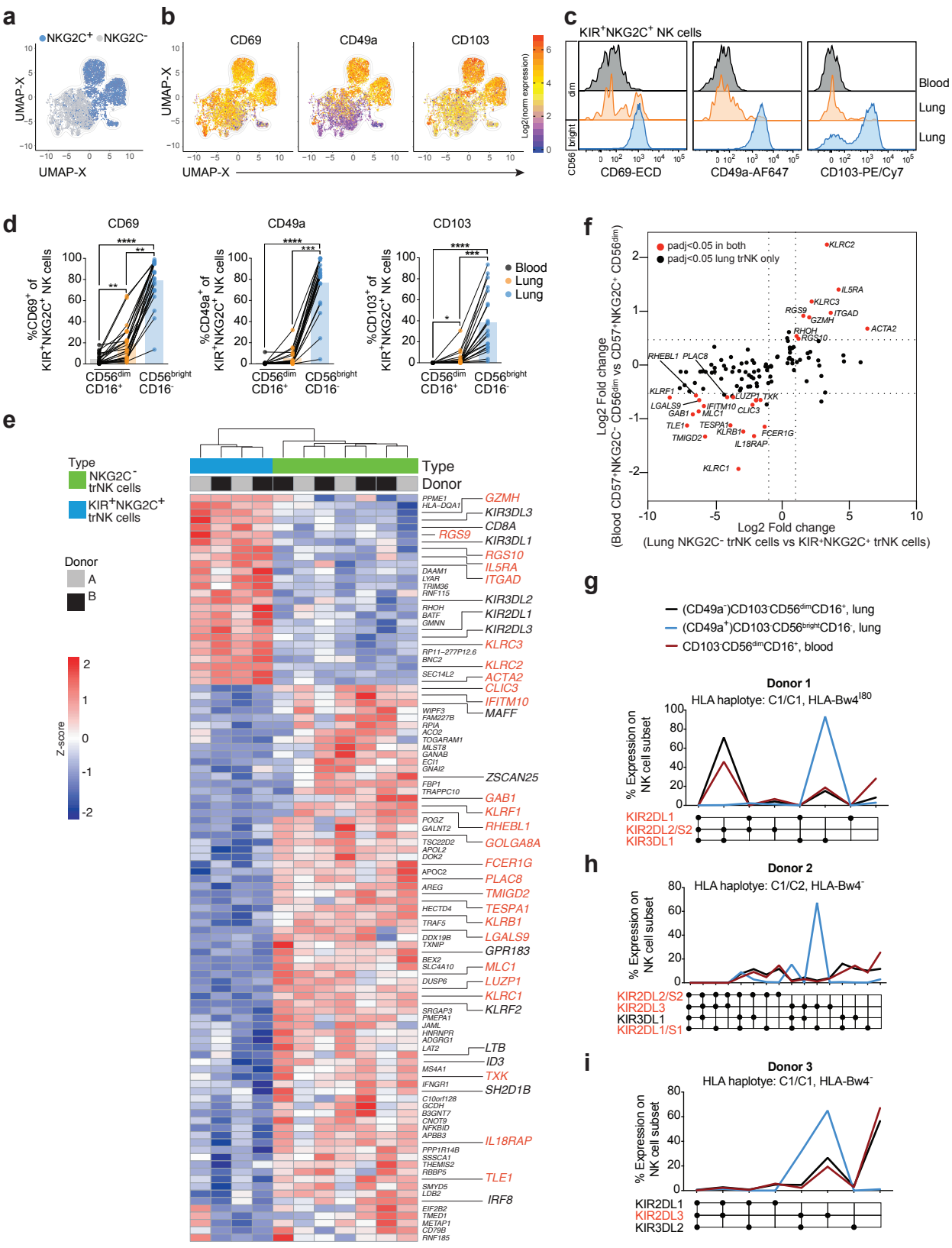

Figure 3

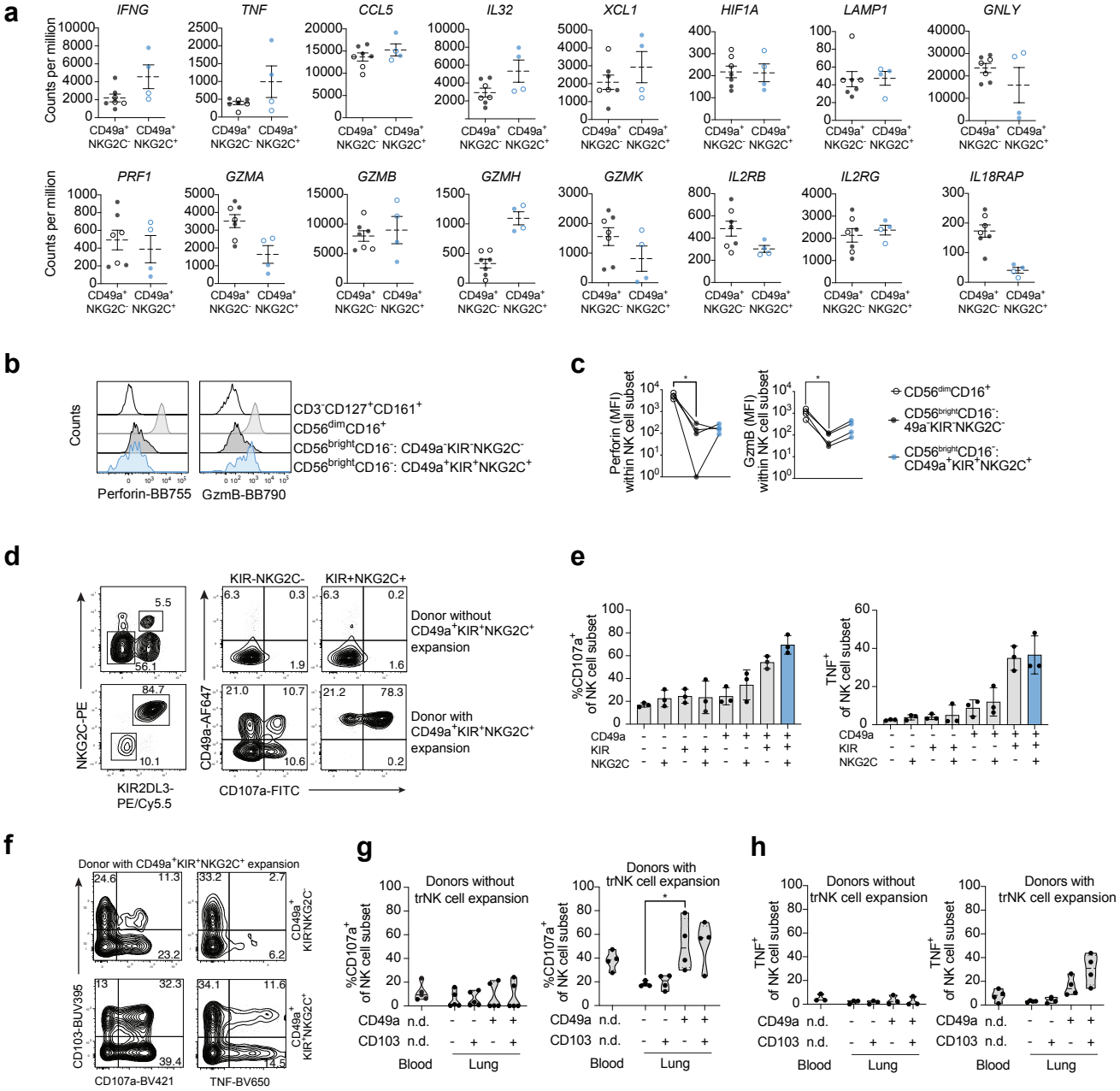

Figure 4

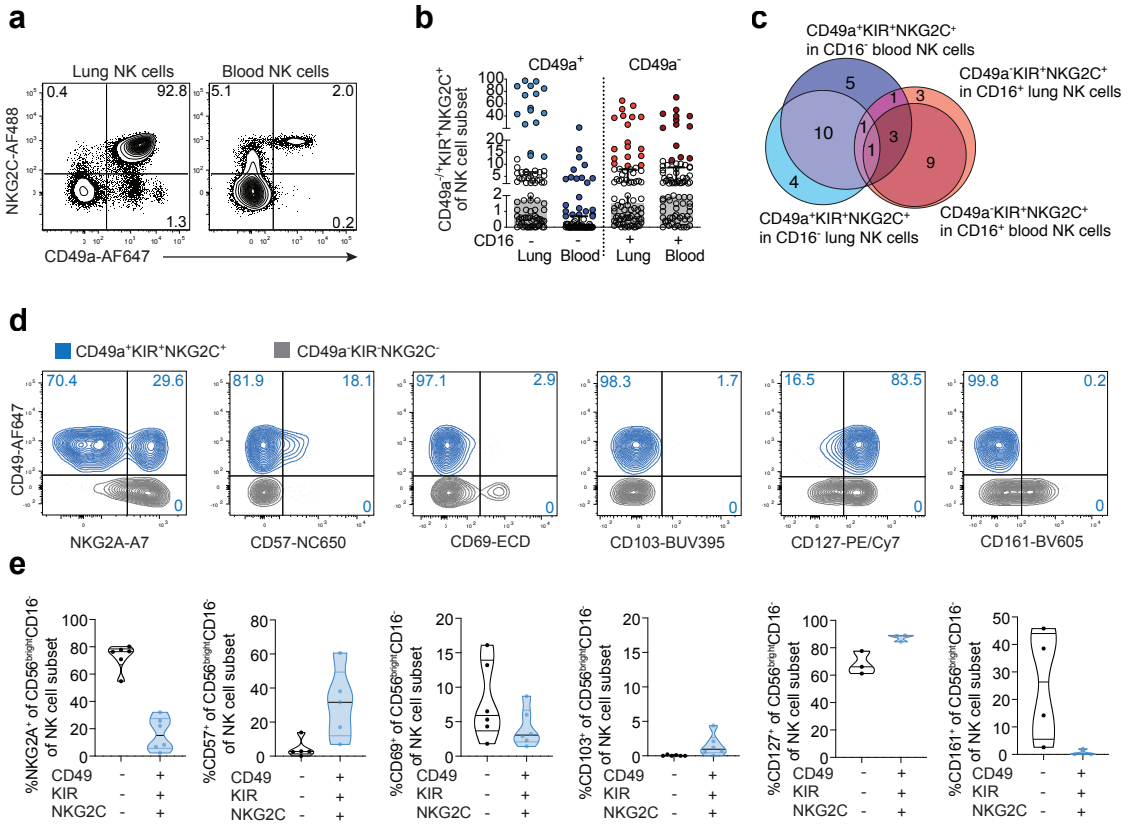

Figure 5

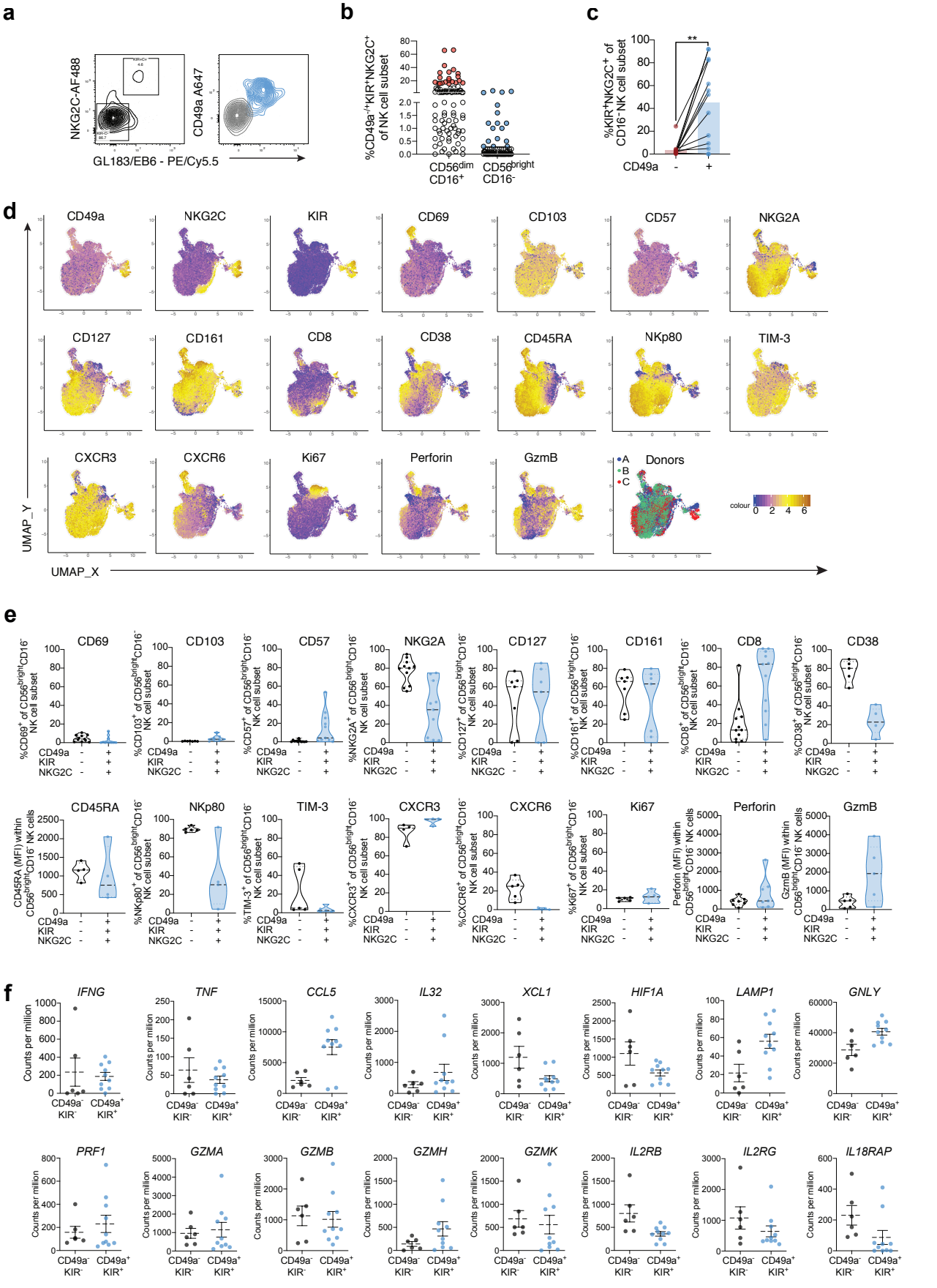

Figure 6

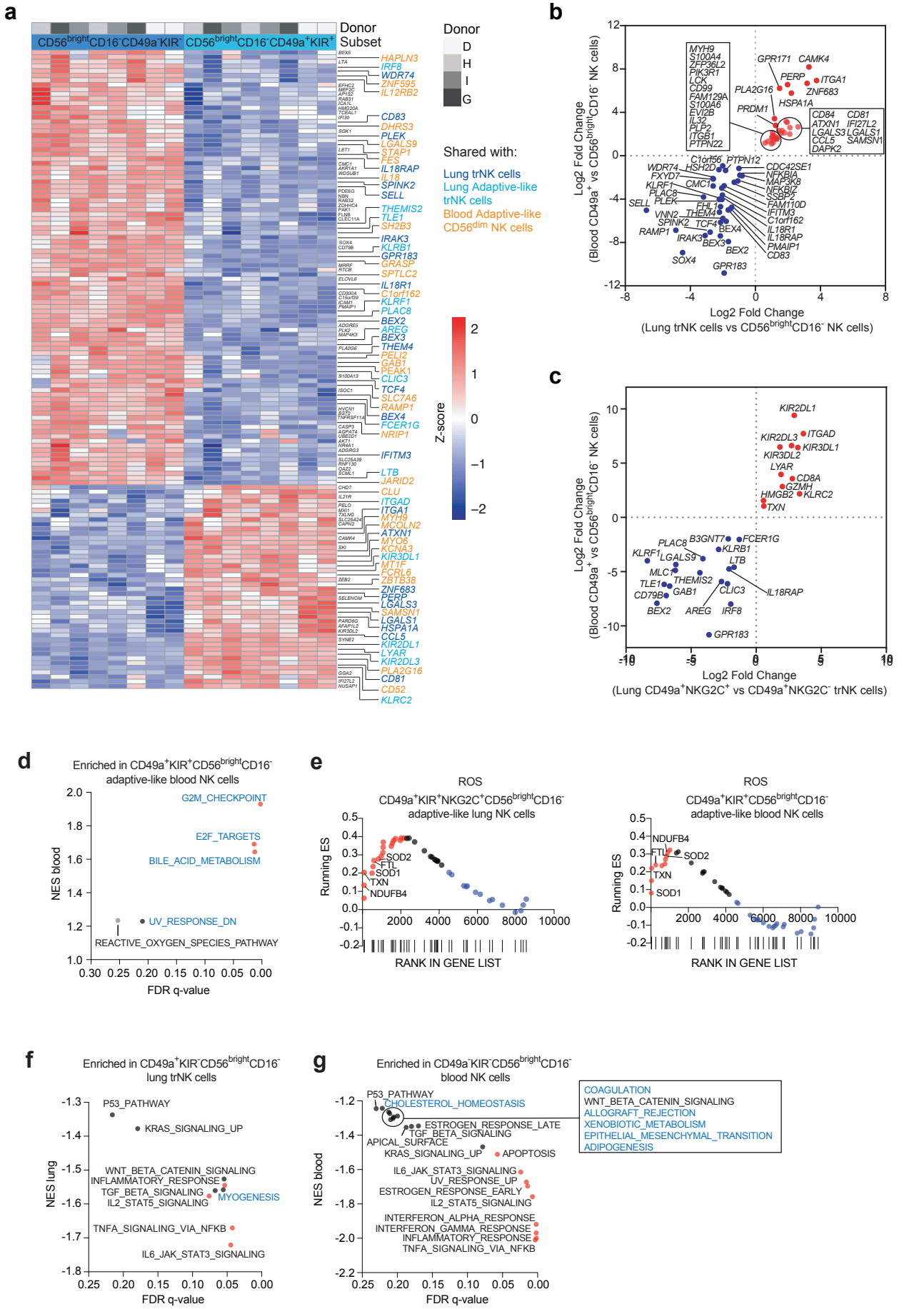

Figure 7

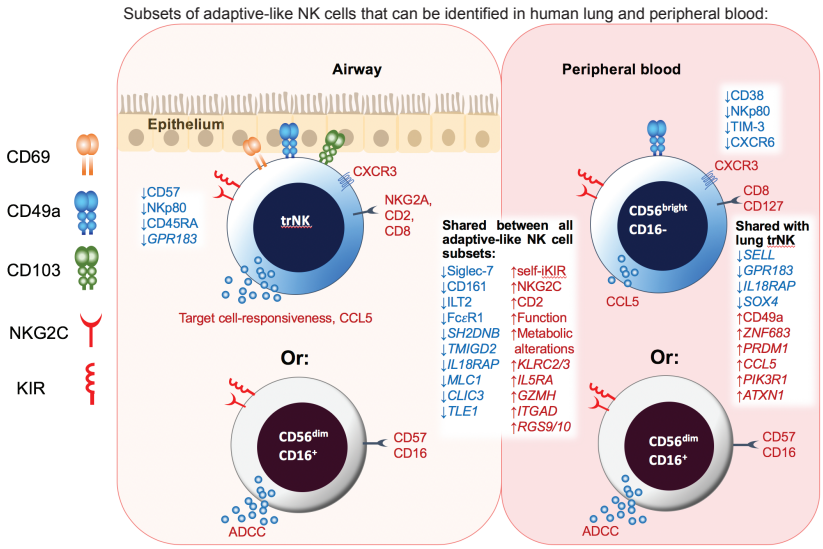

Supplementary Figure 1

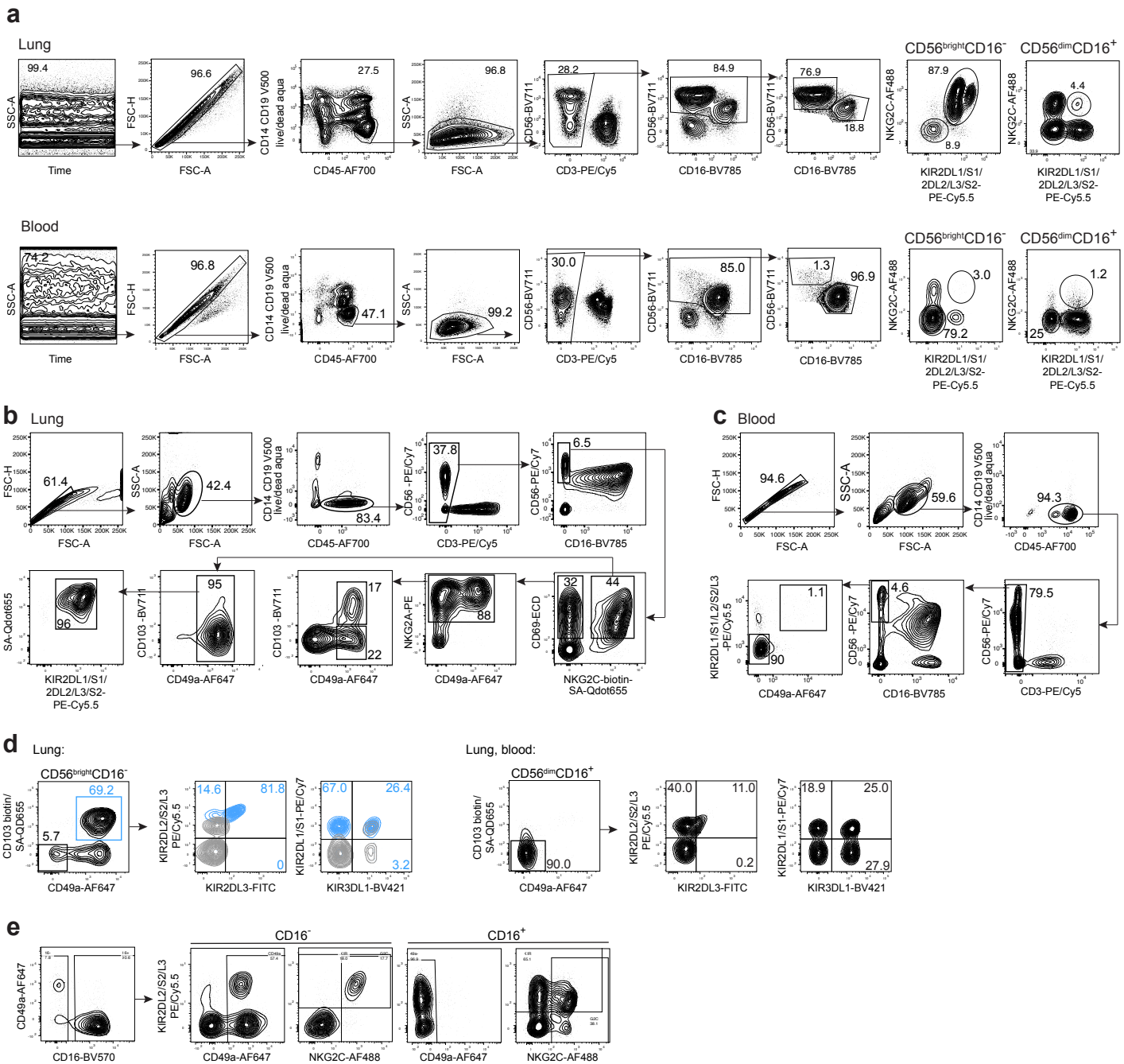

Supplementary Figure 1: Identification of adaptive-like NK cell subsets in human lung and peripheral blood. **(a)** Gating strategy to identify KIR^{+}NKG2C^{+} NK cells in human lung (upper panel) and blood (lower panel) (related to Fig. 1, 2a-d, 3b). **(b)** Gating strategy for sort for RNA sequencing analysis of lung (related to Fig. 2e,f, 3a) and **(c)** healthy blood NK cells (related to Fig. 5f, 6). **(d)** Gating strategy for single KIR analysis on CD56^{bright}CD16^{-} lung NK cells (left panel) and CD56^{dim}CD16^{+} NK cells in lung and blood (right panel) (related to Fig. 2g-i). **(e)** Gating strategy for identification of outliers within the CD16^{-} and CD16^{+} NK cell subsets (related to Fig. 4b,c).

Supplementary Figure 2

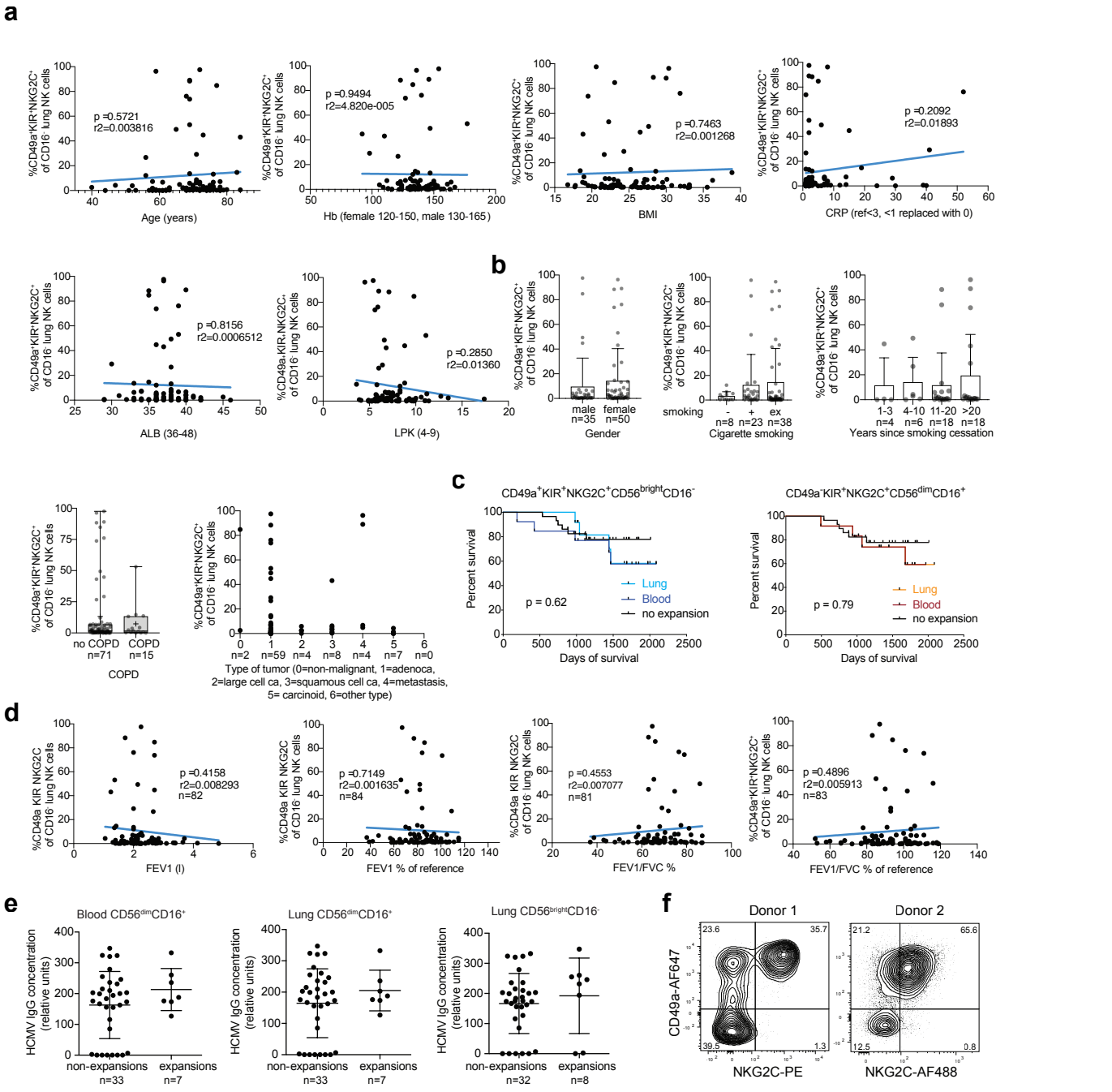

Supplementary figure 2: Association of adaptive trNK cells and patient characteristics. **(a)** Linear regression analysis of the frequency of CD49a^{+}KIR^{+}NKG2C^{+} cells among CD16^{-} lung NK cells versus age, hemoglobin (Hb) levels, body mass index (BMI), c-reactive protein (CRP) levels, albumin (ALB) levels, and leucocyte count (LPK) (n =86). **(b)** Frequencies of CD49a^{+}KIR^{+}NKG2C^{+}NK cells among CD16^{-} lung NK cells versus gender, cigarette smoking status, years since cigarette smoking cessation, chronic obstructive pulmonary disease (COPD) status, and type of tumor. Mean +/- SD is shown. **(c)** Days of survival in donors with CD49a^{+}KIR^{+}NKG2C^{+}CD56^{bright}CD16^{-} NK cell expansions in blood and/or lung (left plot) and in donors with CD49a^{+}KIR^{+}NKG2C^{+}CD56^{bright}CD16^{-} NK cell expansions in blood and/or lung (right plot) (n=57). **(d)** Linear regression analysis of FEV1 (l), FEV1 % of reference, FEV1/FV%, and FEV1/FVC % of reference is shown. **(e)** HCMV IgG concentration in plasma from donors with or without KIR^{+}NKG2C^{+}CD56^{dim}CD16^{+} expansions in blood (left) and lung (middle) and in donors with KIR^{+}NKG2C^{+}CD56^{dim}CD16^{+} expansions in lung (right). **(f)** Expression of NKG2C and CD49a on CD56^{bright}CD16^{-} NK cells from the two HCMV-seronegative donors in (e) demonstrate adaptive-like expansions of CD56^{bright}CD16^{-} NK cells in the absence of HCMV seroconversion.

Supplementary Figure 3

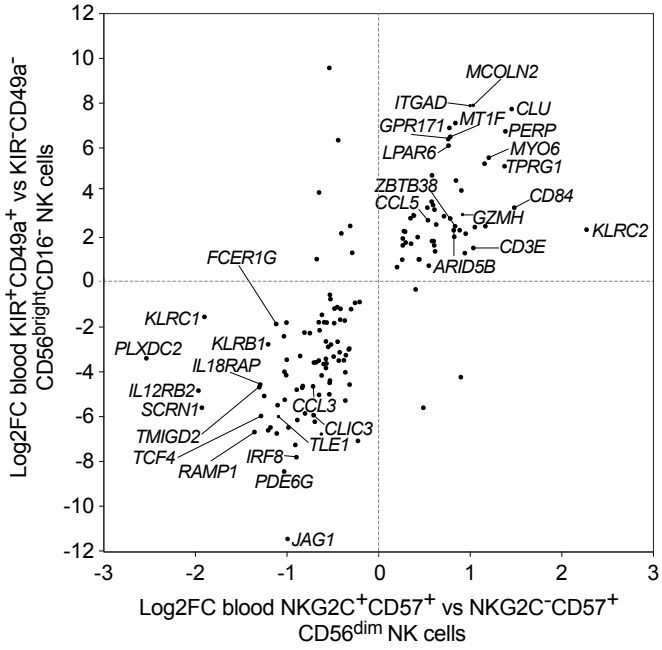

Supplementary Figure 3: Comparison of DEGs between blood CD49a$^+$KIR$^+$ CD56^{bright}CD16$^-$ NK cells and CD57$^+$NKG2C$^+$CD56^{dim} NK cells. Log2-fold changes in gene expression for shared significantly differentially expressed genes between blood CD49a$^+$KIR$^+$ and CD49a$^-$KIR$^-$ CD56^{bright}CD16$^-$ NK cells (y-axis) and CD57$^+$NKG2C$^+$ and CD57$^+$NKG2C$^-$ CD56^{dim} NK cells (x-axis). Data for CD56^{dim} NK cells are from GSE117614 (Cichocki et al).

Supplementary Fig. 4

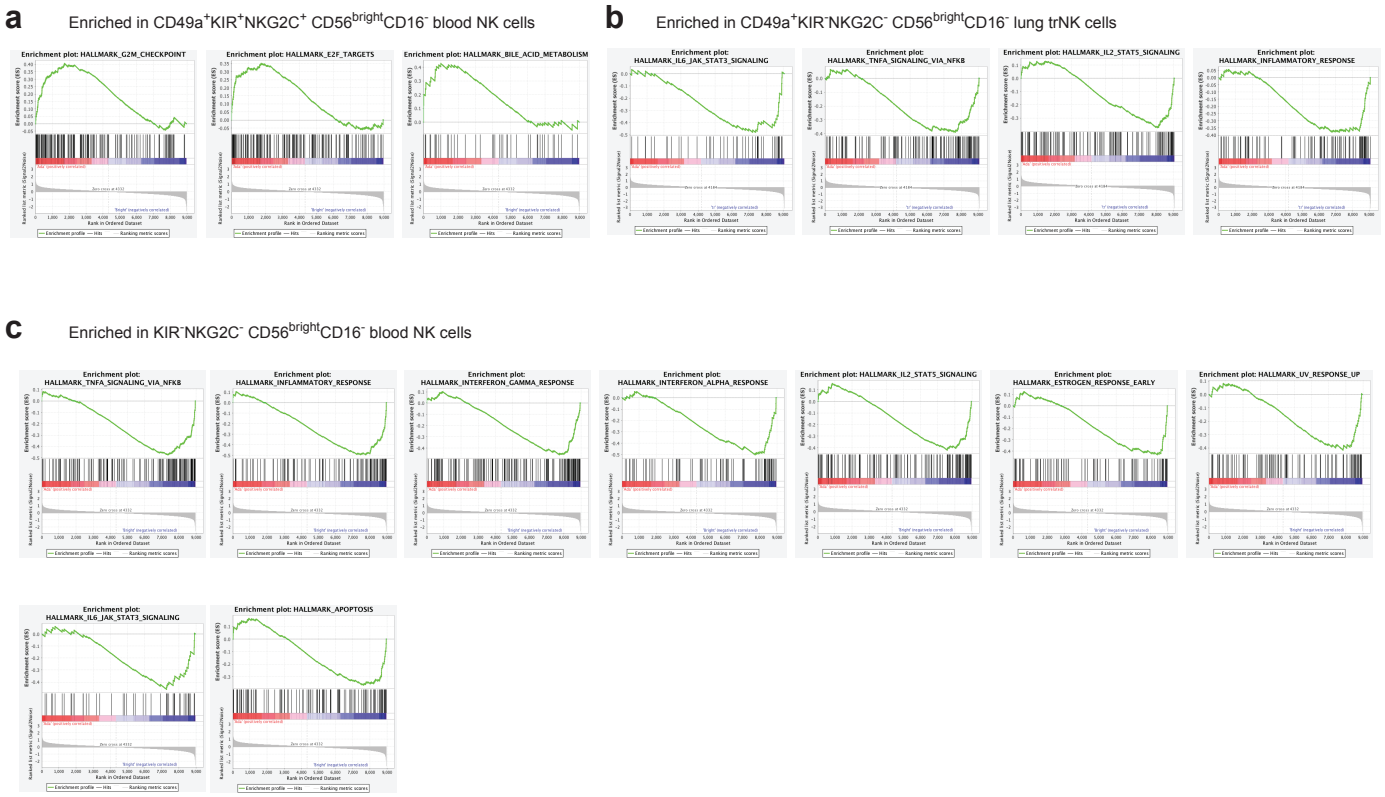

Supplementary Figure 4: Distinct pathways are enriched in adpative-like CD49a^{+}KIR^{+}NKG2C^{+}CD56^{bright}CD16^{-} NK cells in lung and blood at transcript level. (a) Enrichment plots for pathways enriched in CD49a^{+}KIR^{+}NKG2C^{+}CD56^{bright}CD16^{-} adaptive-like blood NK cells. **(b)** Enrichment plots for pathways enriched in CD49a^{-}KIR^{+}NKG2C^{+}CD56^{bright}CD16^{-} (non-adaptive) lung NK cells.**(c)** Enrichment plots for pathways enriched in CD49a^{-}KIR^{-}NKG2C^{-}CD56^{bright}CD16^{-} (non-adaptive) blood NK cells.**(d, e)** Gene expression levels in non-adaptive (CD49a^{+}KIR^{-}NKG2C^{-}CD56^{bright}CD16^{-},CD49a^{-}KIR^{-}NKG2C^{-}CD56^{bright}CD16^{-}) and adaptive-like (CD49a^{+}KIR^{+}NKG2C^{+}CD56^{bright}CD16^{-}) NK cells in lung and blood, respectively, for genes having been reported to be upregulated **(d)** or downregulated **(e)** in cytokine-activated T cells. Mean +/- SEM is shown.